Chapter 6

Graphene for Biosensing Applications

Romaneh Jalilian,[a,b] Luis A. Jauregui,[a,c] Kyuwan Lee,[a,d,e] Yong P. Chen,[a,b,c] and Joseph Irudayaraj[a,d,e]

[a]*Birck Nanotechnology Center,* [b]*Department of Physics,* [c]*School of Electrical and Computer Engineering,* [d]*School of Agricultural and Biological Engineering, and* [e]*Bindley Bioscience Center, Purdue University, West Lafayette, IN 47907, USA*

yongchen@purdue.edu, josephi@purdue.edu

6.1 Introduction

Graphene (a single layer of graphite, although the term is also used to collectively refer to few layers of graphene) is the two-dimensional form of carbon with planar sp^2 bonding. It is also the building block for many carbon nanomaterials, including carbon nanotubes. Since the discovery of electrically isolated graphene in 2004 [1], this novel material has received tremendous interest due to a large number of unique and exceptional properties [2–5]. Many of these properties are highly tunable and sensitively dependent on various parameters. This, along with the fact that graphene is robust and typically exposed to the environment with an extraordinary specific surface area (2620 m^2/g), makes graphene and graphene-based nanomaterials promising as exquisite sensor materials. This review will discuss the fabrication methods, physical/chemical properties, and potential applications of graphene in biosensing, and current status of such research. Work in this area has been scarce but has gained considerable momentum and is expected to grow rapidly in the near future as researchers from diverse disciplines (including biomedical sciences) start to appreciate and utilize the unique properties of graphene for a wide variety of bionanotechnology-related applications.

Biomedical Nanosensors
Edited by Joseph Irudayaraj

ISBN 978-981-4303-03-3 (Hardcover), 978-981-4303-04-0 (eBook)
www.panstanford.com

After a review of current methods in the synthesis of graphene materials and fabrication of graphene devices in Section 6.2, we will review the major physical and chemical properties of graphene in Section 6.3 as a foundation to understanding and developing schemes of sensor operation. Some of the most interesting properties especially relevant to employing graphene in sensors (particularly biosensors) with remarkable functionality and performance are highlighted here:

(1) Exposed to environment with robust properties: Graphene can also behave well in liquid and graphene field-effect transistors (FETs) operating in liquids have been demonstrated [6].
(2) High surface area: 2620 m^2/g for both sides of graphene (e.g., suspended graphene) and 1310 m^2/g for one-side (e.g., supported on a substrate). This also means that a graphene-based composite material can have a huge surface area. This property has also been used to demonstrate, for example, an "ultracapacitor" based on graphene [7].
(3) Graphene (being a sp^2-bonded carbon network) can easily be functionalized to interact with many chemical and biological agents, with the power tool set available from organic chemistry [4, 8].
(4) Excellent electrical properties [9], especially high electrical conductivity and carrier mobility, and ultralow electronic noise: Moreover, many electronic properties of graphene are high *tunable*, including the bandgap, carrier type and density (field effect), and conductivity. Such exceptional and tunable (which can make it sensitive to external perturbations) electronic properties of graphene are appealing for graphene sensors based on conductivity measurement. For example, at room temperature, a graphene sensor that detects the adsorption or desorption of single gaseous molecules has been demonstrated [10] based on the extraordinary sensitivity of graphene to local electrical perturbation.
(5) Unique optical properties: Graphene is largely transparent (despite being highly conductive) [11, 12], with many distinctive optical properties and spectroscopic signatures (e.g., Raman [13]). These properties also often affected by external perturbations and may be utilized in optical-based sensing. Moreover, graphene has been shown to be able to strongly influence the optical/spectroscopic properties of objects (e.g., molecules) adsorbed on it [14, 15], opening many opportunities for sensing.

Other appealing properties of graphene as a sensor material include high thermal conductivity [16], excellent mechanical properties [17, 18], and relative ease of planar patterning using standard micro/nano fabrication (offering outstanding potentials to develop miniaturized sensors with high spatial resolution).

In Section 6.4 of this review, we will discuss how graphene may be affected by (or affect) external objects or environmental "stimuli" for sensing applications (including particularly, but not limited to, biosensing). From a fundamental point of view, graphene can be thought of both as a giant carbon molecule and a two-dimensional solid-state system possessing both types of properties while not completely described by either point of view alone. This places graphene in a unique position to interact with other molecular or nanoscale objects (e.g., biomolecules) and create responses in a measurable way, making graphene an exceptionally appealing sensor material. For example, recent experiments

have shown that the electrical property of graphene can be affected by biological objects on its surface [19] and graphene can serve as a platform to detect biomolecules and interactions (e.g., binding/unbinding) optically [14].

The last section (Section 6.5) will give some closing remarks and present some promising future directions in the study of graphene and its employment for biosensing applications.

6.2 Fabrication of Graphene-Based Materials and Devices

6.2.1 Graphene Materials Fabrication

The most common method to fabricate graphene is by mechanical exfoliation [1, 20] from graphite onto a substrate (e.g., silicon wafer). This straightforward method, which typically gives graphene flakes with relatively small size (<100 μm), is best suited to make single devices to perform fundamental studies and proof-of-concept experiments. An extension of this method by nanoimprinting [21] promises to make arrays of many graphene devices over a large area. Graphene can also be synthesized on a variety of substrates, including silicon carbide (SiC) by thermal decomposition [22] and transition metals by chemical vapor deposition (CVD) or surface segregation [23, 24]. These synthetic methods are particularly interesting for growing graphene on a large scale for practical applications. In addition, a large number of "graphene-based" materials can be synthesized by various methods from (often chemically functionalized) graphene sheets and their mixture with other materials (such as in a composite) to fulfill certain functions.

Micromechanical exfoliation (cleavage) of bulk graphite was the first technique that allowed the deposition of (electrically) isolated graphene on a substrate. This method is simply repeated by peeling off graphite with adhesive tapes until the thinnest flakes are found and transferred to a substrate by the physical contact of tape and the substrate [20], as demonstrated in Fig. 6.1.

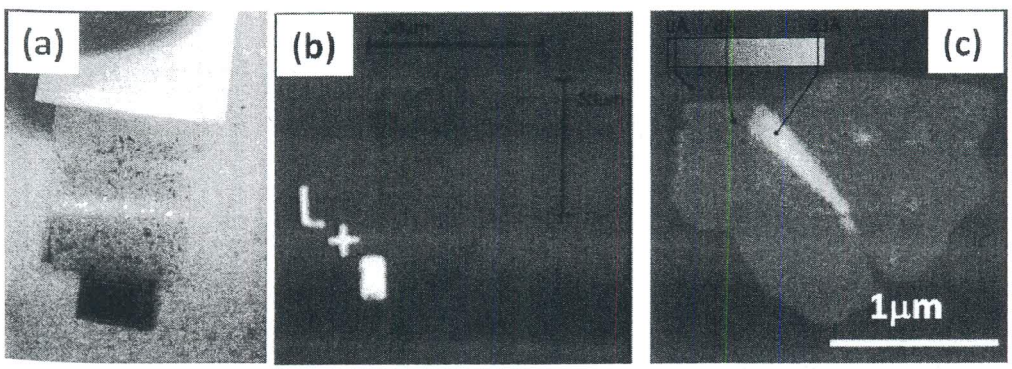

Figure 6.1 (a) Mechanical exfoliation of graphene using scotch tape (b) optical and (c) atomic force microscope (AFM) image of a peeled single layer of graphene. (Figure (c) Reprinted with permission from ref. 20.)

Several more sophisticated exfoliation methods have been developed. Electrostatic deposition of loosely bonded graphene flakes from highly oriented pyrolytic graphite (HOPG) is another alternative method for extracting graphene from graphite [25]. Liang *et al.* demonstrated graphene exfoliation using pillars on a stamp and then used the transfer printing method to place the exfoliated islands of graphene to a device-active area on a substrate [21]. Also, incorporating the electrostatic deposition and stamp technique, Liang reported electrostatic exfoliation of nanometer to micrometer-sized few-layer graphene (FLG) from patterned HOPG onto substrates [26]. Many methods have also been developed to perform chemical and/or solution-assisted exfoliation of graphite to extract graphene or chemically modified graphene (CMG) [27, 28].

Another technique for fabricating graphene is by the sublimation of Si from the SiC surface to produce epitaxial graphene sheets on SiC (a semiconductor) [22, 29] (Fig. 6.2). Prior to growth, substrates are typically etched in hydrogen. The temperature required for the growth of graphene film ranges from 1,350–1,650°C. At such high temperatures, Si atoms leave the surface, and graphitization occurs. The quality and thickness of graphene layers grown depend on many parameters, including which surface of SiC is used. More recently, it has become possible to grow large-area monolayer graphene epitaxially on SiC [30].

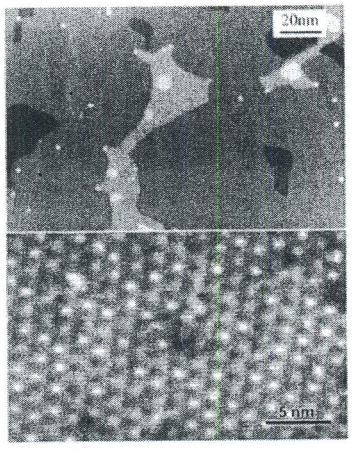

Figure 6.2 Scanning tunneling microscope (STM) images of epitaxial graphene growth on SiC. (Reprinted with permission from ref. 29).

Another method to synthesize graphene is by CVD growth on metal surfaces. This is a decades-old technique [24, 31]. Recently, it has been demonstrated that such growth performed on copper foils [23, 32] is particularly successful in producing large-size monolayer graphene (reaching 30 inches in size [33]) that can be transferred to arbitrary substrates (including flexible substrates). The graphene grows as film directly on the copper surface by a surface-catalyzed CVD process, at temperatures up to 1,000°C and low or ambient pressure, by the extraction of carbon from the decomposition of hydrocarbons (e.g., methane) [23, 34]. This growth is also successful on thin (on the order of 100 nm in thickness) copper films on solid substrates as well [35]. Also, large-area graphene films can be synthesized by the surface segregation of carbon atoms (dissolved from decomposed hydrocarbon gases) from Ni under the ambient pressure followed by cooling down from high temperatures. The hydrocarbon molecules decompose at the Ni surface, and carbon

atoms diffuse into the metal. Using appropriate cooling rates, carbon atoms can segregate at the surface to form graphene layers [36]. Large-size transferrable graphene films (most often containing a mixture of monolayer and multilayer) have been grown by such a method on Ni foils [36, 37] and Ni thin films [38, 39]. Various examples of metal-based CVD growth of graphene are shown in Fig. 6.3.

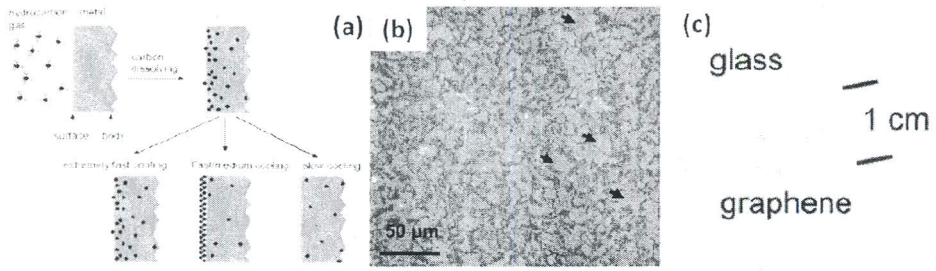

Figure 6.3 (a) A schematic representation of hydrocarbon decomposition, carbon deposition (on surface), dissolution (into metal), and various segregation/diffusion behavior upon cooling; (b) and optical image of CVD graphene grown using Ni film consisting of one to two layers of graphene (the black arrows); (c) monolayer CVD graphene film grown on Cu and then transferred onto a glass plate. (Fig. 6.3a, b, and c reprinted with permission from ref. 36, 39, and 23, respectively.) See also Color Insert.

Another route to synthesize graphene is by the chemical reduction of graphene oxide (GO) [40, 41] as graphite oxide (synthesized by oxidizing graphite with acids) is water soluble and much easier to exfoliate [8]. GO is hydrophilic (in contrast to graphene, which is hydrophobic), allowing stable aqueous dispersion in water. It is convenient to exfoliate GO into nano-sized single layers, which is the promising mass production of both GO and graphene. Using such a method, one often obtains partially oxidized graphene or graphene with a chemical functional group attached. Various methods are being also developed to exfoliate graphite in solutions with appropriate chemical properties [8, 27] to obtain graphene or chemically functionalized graphene.

In addition to graphene thin films (single or few atomic layers), graphene-based conducting composites [42] have been successfully demonstrated, where a relatively large amount (several percent of volume fraction) of graphene flakes is dispersed in a polymer (e.g., polysterene) matrix to make a macroscopic, solid form of composite (which is conductive due to a graphene network) with excellent material and electronic properties and a large surface area, which may be particularly interesting for sensing applications.

6.2.2 Graphene Device Fabrication

We briefly describe here the typical lithography fabrication process of a graphene device with electrical connection. Graphene is placed (by exfoliation or other ways of transfer) on a degenerately doped Si substrate with an oxide overlayer (Fig. 6.4). The doped Si substrate can be used as a back gate to tune the carrier type and concentration in graphene by an electric field effect (see Section 6.3). The electric contact leads on graphene are fabricated by e-beam and/or optical lithography. The fabrication steps are presented in Fig. 6.4 (a–e). Also, by etching the SiO_2 underneath graphene after the fabrication of the graphene sensor, it is possible to make suspended graphene. The change of graphene electrical property

integrated into a device can be measured due to its chemical, physical, and mechanical responses to changes in the surrounding environment.

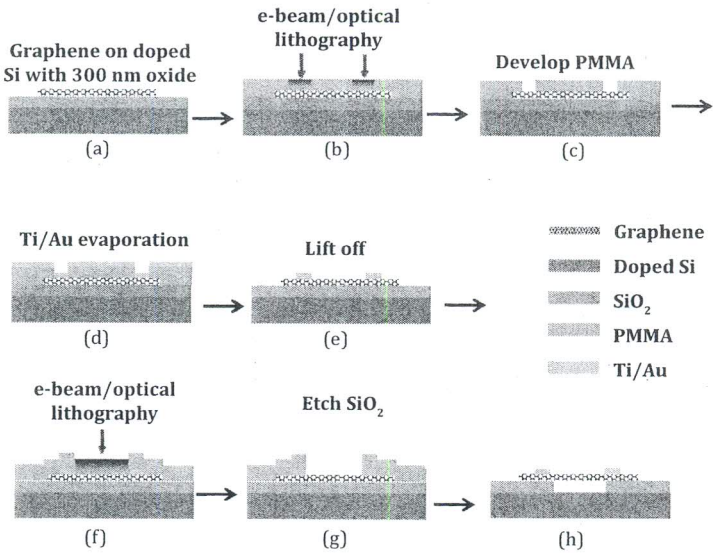

Figure 6.4 (a) Graphene deposition, (b) e-beam/optical lithography, (c) developing exposed regions on e-beam/photo resist (poly[methyl methacrylate], or PMMA, is an example of e-beam resist), (d) metal evaporation, and (e) lift off. To suspend the graphene in the device, (f) second e-beam optical lithography opening a window over graphene, (g) wet etching of SiO_2 by hydrofluoric acid, and (h) remove the extra photo/e-beam resist and dry the sample by a critical point dryer. See also Color Insert.

6.3 Basic Properties of Graphene

Graphene is formed by sp^2 carbon-carbon bonds in a honeycomb shape. The unit cell is formed by two carbon atoms (referred to as atom A and atom B). Figure 6.5 shows the representation of a graphene sheet and its respective unit cell.

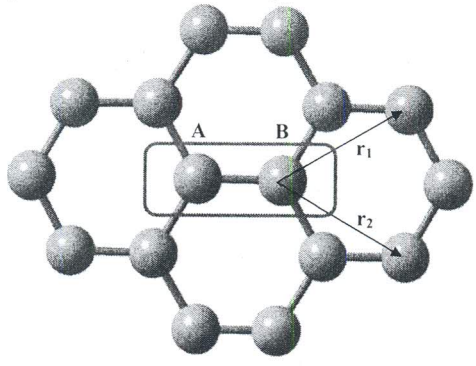

Figure 6.5 A portion of a graphene sheet; each light-blue ball is a carbon atom, and the sticks are the representation of the sp^2-bonds between carbon atoms. One cite in a unit cell of graphene is marked by a red hallmark. See also Color Insert.

6.3.1 Electrical Properties

As an electronic material, graphene has the highest mobility at room temperature among all known materials. For this reason, graphene has been considered as one of the most promising material for "post-silicon" (beyond Moore's law) electronics in semiconductor industry and much work has started to explore the applications of graphene in high-speed, high-performance, and low-power electronic devices.

The electronic band structure of graphene can be constructed using the tight-binding method; the size of this matrix will depend on the number of valence orbitals. Carbon has six electrons in total. There are four electrons in the valence band, and four basis functions (2s, $2p_x$, $2p_y$, and $2p_z$) will be needed to represent each carbon atom. However, the unit cell is formed by two carbon atoms; therefore, eight basis functions will be necessary per unit cell [43]. It is interesting to point out that the levels related to the orbitals 2s, $2p_x$ and $2p_y$ are far separated from the Fermi energy compared to the levels related to the orbitals $2p_z$. Therefore, the conduction is mostly related to the levels related to the $2p_z$ orbitals, simplifying the number of basis functions to just two needed per unit cell. Solving the Hamiltonian describing electrons moving in the graphene lattice, a linear relation between momentum ($p = \hbar k$) and electron energy (E) is obtained:

$$E = v_F p = \hbar v_F k \text{ , where } v_F = 10^6 \text{ m/s is called the Fermi velocity.}$$

One of the most striking differences between this result from graphene compared to other semiconductors is that here, E is just linear dependent with k, leading to a constant velocity, called Fermi velocity, with an effective mass equal to zero. This Fermi velocity does not depend on energy or momentum, while in other semiconductors, the Fermi velocity depends on the root square of energy and there is a finite effective mass for electrons. The constant velocity plays a similar role as the speed of light in usual relativistic massless particles as photons. This unique energy-momentum dispersion of charge carriers and a nonzero Berry's phase [44] related to the lattice structure (A and B atoms being symmetric) have important implications for the electronic transport of carbon materials, including graphene and single-walled carbon nanotubes (SWCNT, which are rolled-up graphene sheets).

Experiments have shown mean free paths for graphene and SWCNT as long as ~10 μm at low temperatures (20 K) and ~1 μm at room temperature [45], showing that ballistic devices working at room temperature can be made for microscale devices. This ballistic behavior at room temperature is a direct consequence of the nonzero Berry's phase happening in graphene that protects electrons from being scattered.

Both the type and density of charge carriers in graphene can be tuned by an electric field (provided by, for example, a gate voltage). Varying the carrier density tunes the conductivity of graphene, resulting in a field effect device [1]. The typical dependence of resistivity on the gate voltage for graphene devices has a sharp peak on the order of kilo-ohms, while the resistivity drops far away from this peak to hundreds of ohms (Fig. 6.6). The gate voltage induces a surface charge density, which shifts the position of the Fermi level in the graphene. This electric field can transform the graphene channel into either completely n-type (electron) or completely p-type (hole) conductor and a mixed state where both electrons and holes are present; this behavior is called an ambipolar

electric field effect. A positive (negative) back-gate voltage induces electrons (holes) in concentrations proportional to the back-gate voltage value [1].

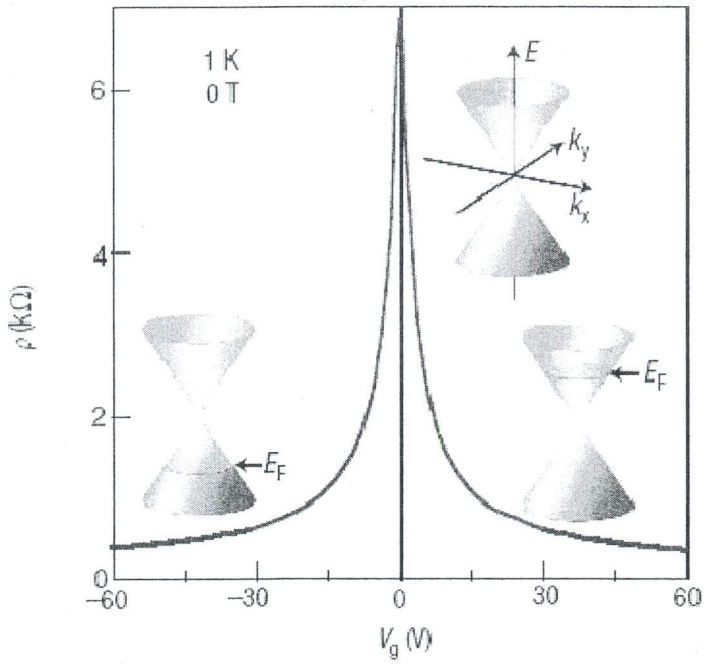

Figure 6.6 The ambipolar effect in graphene devices. The Fermi level changes when the back gate is applied from a negative to a positive value. (Reprinted with permission from ref. 5.)

The sharp peak in Fig. 6.6 is called the Dirac point. An important observation in graphene is that the conductivity of graphene at zero charge density (Dirac point) doesn't vanish; instead, it approaches a value on the similar order of the quantum conductance $4e^2/h$ [46]. Near the Dirac point, the resistivity (inverse of conductivity) is very sensitive to even a small and *local* change in the carrier density [10], or a local electrostatic potential. This can be a key mechanism for novel schemes of using graphene to detect charges or electric fields in biological systems.

Moreover, often the position of the neutrality point (Dirac point) as well as the carrier mobility of graphene is dependent on external doping, which in term can depend on the local environment of graphene [47, 48]. Chen *et al.* [47] doped graphene by potassium atoms under ultrahigh vacuum; the minimum of conductivity depended on the charged-impurity density, and the carrier mobility decreases with an increase of charge impurity density; but these are reversible by heating the sample to remove the potassium atoms. Schedin *et al.* [48] doped graphene with NO_2, H_2O, I, NH_3, CO, and ethanol, showing that the first three gases acted as acceptors while the last three compounds acted as donors.

Electronic noise is an important issue for sensor operation. Graphene is a highly conductive material with a zero electronic bandgap (metallic conductivity), leading to a low Johnson noise even at low charge densities (near the Dirac point) and at room

temperatures. These properties make graphene an exceptional electronic low-noise material [10]. Coupled with graphene high sensitivity to a change in charge density or an applied external field near the charge neutrality point (Dirac point) enables such a high signal-to-noise ratio that makes graphene sensors capable of detecting change in the local charge concentration by less than 1 electron [10]. Based on such a principle, a room-temperature graphene sensor that detects adsorption or desorption of single molecules has been recently demonstrated [10]. Graphene typically has a small amount of crystal defects [20, 46, 48, 49], which can lead to a low level of pink ($1/f$) noise. Two sheets of graphene stacked together (as in graphite), known as bilayer graphene, have also been studied by Lin *et al.* [50] who found that bilayer graphene has in particular a lower noise figure than single-layer graphene, even lower than the Johnson noise limit. Figure 6.7 shows that a bilayer graphene device has a smoother resistance-gate voltage response compared to the single-layer device and bilayer graphene resistivity around the Dirac point is smaller than in a single layer. These observations lead us to think and demonstrate that bilayer graphene devices are less noisy than single-layer graphene ones. The power spectral density was measured on several devices with different geometries; the noise figure versus resistance over length is depicted in Fig. 6.7. As shown in Fig. 6.7, the noise characteristic for a single-layer device is constant for different resistances. However, bilayer devices possess lower noise than single-layer ones, with a decreasing noise characteristic when the resistance is increased.

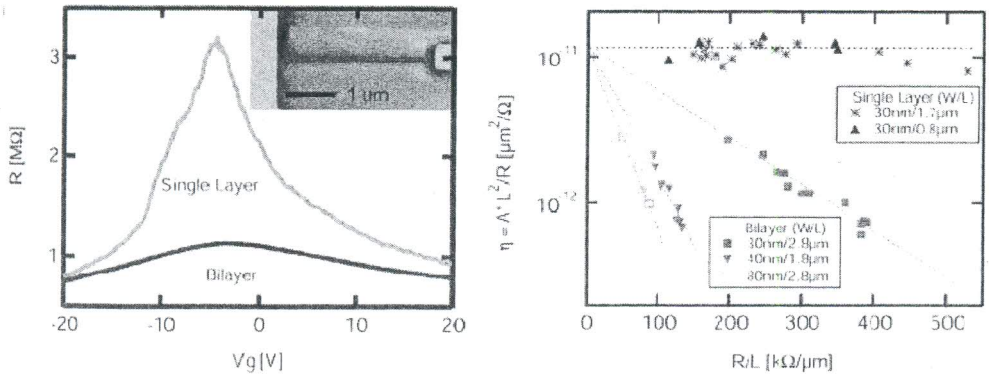

Figure 6.7 (a) Back-gate voltage sweep for single- and double-layer graphene devices with the same geometrical dimensions, showing a smoother signal for bilayer graphene compared to single-layer graphene; (b) noise figure versus resistance/length for single- and double-layer graphene devices. (Reprinted with permission from ref. 50.)

The electronic properties of graphene as noise or carrier mobility are highly dependent on the interaction with the substrate, commonly SiO_2. This dependence can be shown by removing the substrate. Bolotin *et al.* [51] and Du *et al.* [52] found that after suspending a single layer graphene sheet (Fig. 6.8) by removing the substrate, the carrier mobility of graphene increases from values ranging between 2,000 $cm^2 V^{-1}s^{-1}$ and 25,000 $cm^2 V^{-1}s^{-1}$ to values reaching 60,000–230,000 $cm^2 V^{-1}s^{-1}$ after current-induced annealing.

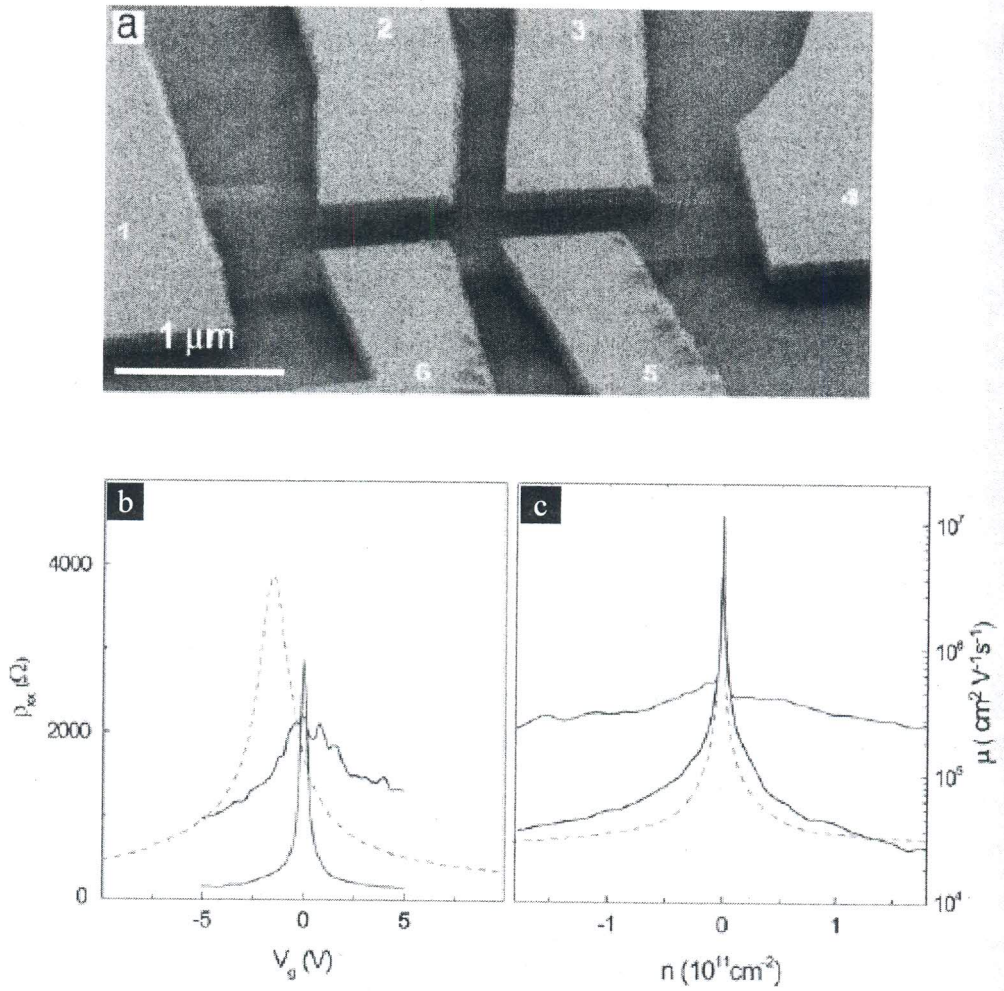

Figure 6.8 (a) SEM on a suspended graphene device; (b) resistance between leads 1 and 4 versus the voltage applied to the back gate; (c) calculated mobility versus charge density modulated through the back gate. (Reprinted with permission from ref. 51.)

The electrical properties of nonsuspended and suspended graphene depend on the temperature, as can be seen in Fig. 6.9a, where the relative change of resistivity normalized by the room temperature value ($\rho(T)/\rho(300\ \mathrm{K})$) is plotted for two representative carrier densities $n = 0$ (Dirac point) and $n = 3 \times 10^{12}\ \mathrm{cm}^{-2}$ (high density). A metallic behavior (monotonic reduction of $\rho(T)/\rho(300\ \mathrm{K})$ for a decreasing temperature) is observed, interpreted by that the residual electron-phonon scattering is part of the scattering mechanism in the high-density limit of conduction. However, for $V_g - V_{\mathrm{Dirac}} = 0$ (Dirac point), the resistivity increases with a decreasing temperature, indicating nonmetallic behavior

of the carriers at the Dirac point [53] for this moderate-mobility sample (unsuspended). For high-mobility suspended [51, 54] or unsuspended [55] graphene devices, metallic behavior can be found at all densities. As shown in Fig. 6.9b, the temperature dependence is also sample dependent, suggesting that the transport at the charge neutrality point (Dirac point) is dominated by extrinsic scattering [56].

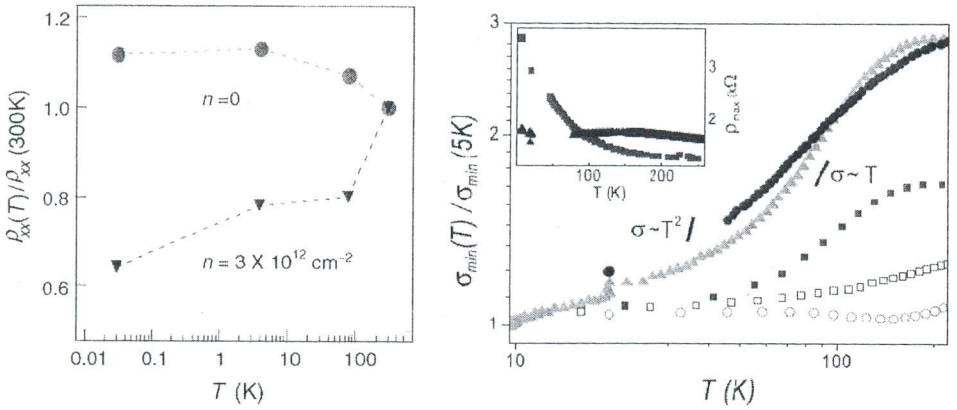

(a) (b)

Figure 6.9 (a) $\rho(T)/\rho(300\ \text{K})$ at two different densities, Dirac point ($n = 0$) and high density ($n = 3 \times 10^{12}$), for a moderate mobility (nonsuspended) graphene device [57]. (b) $\sigma_{min}(T)/\sigma_{min}(5\ \text{K})$ at the Dirac point for high-mobility (suspended) graphene devices, as a function of T for three devices before (S1□ , S2 ○) and after (S1 ■, S2 ●, S3 ▲) annealing. (Reprinted with permission from ref. 54.) See also Color Insert.

Intrinsically, graphene is a zero bandgap semiconductor (semimetal), which means graphene is always in the "ON" state. For many sensors or transistor applications, we need to switch from the "ON" to the "OFF" state. Many researchers have been working on opening a bandgap in graphene. And a bandgap can be opened by various procedures or mechanisms: geometric confinement/patterning (e.g., nanoribbons [28, 58] or antidotes [59]), electric field in bilayer graphene [60], interaction with substrate [61], or controlled oxidation [62]. Most of the bandgap reached so far ranges from 0 to 0.4 eV.

Graphene nanoribbons (GNR) are strips of graphene that are obtained by geometric confinement/patterning. These strips can be armchair or zigzag, depending on their edge structure. Calculations show zigzag GNRs are always metallic; in contrast, armchair GNRs are semiconducting, with a bandgap inversely proportional to its width [63]. Han *et al.* [64] and Chen *et al.* [65] studied how an apparent bandgap is opened in graphene nanoribbons with rough edges for different ribbon widths as it can be visualized in Fig. 6.10, where the measured bandgap increases for a decrease in the width of the nanoribbons. Han *et al.* reported a 300 meV bandgap induced for ~15 nm wide graphene nanoribbons. Pedersen *et al.* modeled a periodic array of holes (antidote lattice) in graphene to show that such an artificial nanomaterial can be controlled to create a bandgap with a very pronounced optical-absorption edge [59].

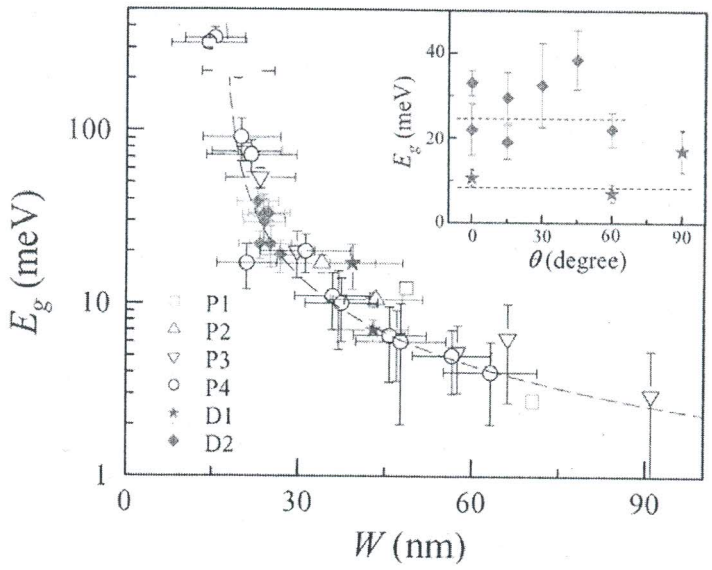

Figure 6.10 The bandgap opened in graphene nanoribbons versus the width of the nanoribbons. (Reprinted with permission from ref. 58.)

An electric field can open a bandgap in bilayer graphene devices. Oostinga *et al.* [66] used a double-gate (back-gate and top-gate electrodes) bilayer graphene FET device, which induces a chemical potential difference between each of the graphene layers and opens a bandgap as can be seen in Fig. 6.11. They could open a small bandgap close to 10 meV.

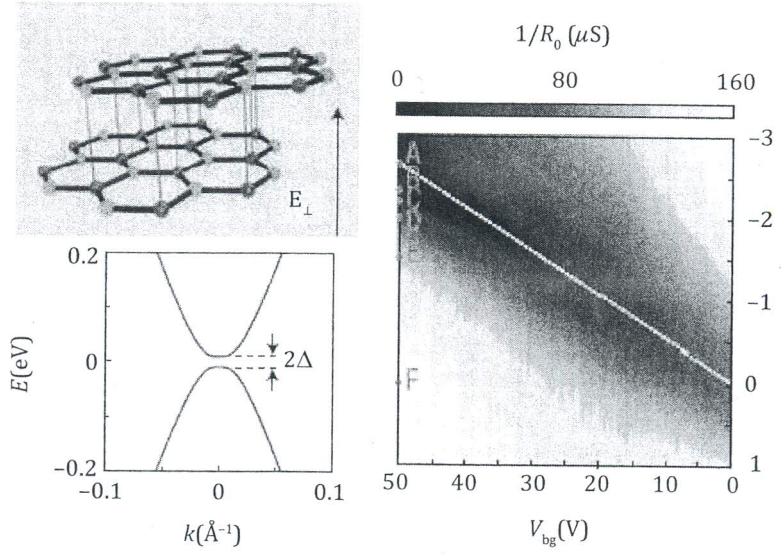

Figure 6.11 A bandgap opening in bilayer graphene by a perpendicular electrical field applied using a top-gated device. (Reprinted with permission from ref. 60.)

Another way to create a bandgap in graphene was shown by Zhou *et al.* [67] on epitaxially grown graphene on SiC grown. A bandgap of ~0.26 eV was measured on these samples. The proposed origin of this bandgap opening is the breaking of A-B site symmetry due to the graphene-substrate interaction.

6.3.2 Optical Properties

We will briefly review the optical properties of graphene, an understanding of which is critical for developing sensor devices. First, understanding the optical visibility of graphene using its optical contrast is essential for imaging, as well as for interrogating the number of layers. Graphene has much stronger visibility in reflection than transmission. Especially, when the bare substrate thickness is appropriate to achieve the resonant light transmission, the visibility of graphene reaches the optimum conditions [68]. It is because the interaction of light with electrons in graphene renders graphene relatively opaque in spite of its monolayer structure [69]. In other words, while the transparent substrate is transmitting the light, graphene reflects a certain amount of light and this makes graphene visible under a normal microscope. Therefore, it is necessary to consider the type of substrate that will be used to acquire a clear image of graphene.

As a direct result of Fresnel's theory, the light intensity reflected from graphene can be written as [70]:

$$I(n_1)=\left|\frac{r_1e^{i(\phi_1+\phi_2)}+r_2e^{-i(\phi_1-\phi_2)}+r_3e^{-i(\phi_1+\phi_2)}+r_1r_2r_3e^{i(\phi_1-\phi_2)}}{r_1r_2e^{-i(\phi_1-\phi_2)}+r_2r_3e^{i(\phi_1-\phi_2)}+r_3r_1e^{-i(\phi_1+\phi_2)}+e^{i(\phi_1+\phi_2)}}\right|^2 \tag{6.1}$$

where $r_i = (n_{i-1} - n_i)/(n_{i-1} + n_i)$ is the index of refraction, I is the intensity of light, n is the refractive index, and $\phi = 2\pi nd/\lambda$ is the phase shift, respectively.

By definition, the contrast C is described as

$$C=\frac{I(n_1=1)-I(n_1)}{I(n_1=1)} \tag{6.2}$$

For optimum visibility, the wavelength of monochromatic light used should meet the resonance condition of the substrate combining Eq. (6.1) and (6.2), and the bilayer gives a better visibility than the monolayer in the visual frequency range of the light source.

While light reflection provides better visibility of graphene, transmission is also very interesting when graphene is to be used in many optical devices such as liquid crystal displays or transparent electrodes. This is because graphene has low resistivity, high transparency, and chemical stability compared to other metal oxides [72]. Naturally, the transmission of graphene doesn't depend on the substrate thickness. Even suspended single-layer graphene can be solely identified by transmission due to graphene's unique electronic structure. Light is interacting with relativistic electrons (with linear energy-momentum dispersion) in graphene, and the opacity of graphene is determined only by the fine structure constant $\alpha = 2\pi e^2/hc \sim 1/137$. This is a universal characteristic of quantum electrodynamics of two-dimensional Dirac electrons regardless of material parameters. This is why graphene absorbs a sizable amount of light ($\pi\alpha = 2.3\%$) in spite of its single-atomic-layer structure. The experimental result agrees with the above theoretical expectation from two-dimensional Dirac electrons calculated with Fermi's golden rule.

This optical property of graphene is related to its electrical property showing a universal dynamic conductivity over visible frequencies due to the behavior of ideal Dirac electrons [12] (Fig. 6.13). This can be directly used not only for counting the number of layers but also for optical device replacing other metal oxides because graphene is an excellent transparent and conductive material with good chemical stability. For example, Blake *et al.* demonstrated that it can replace indium tin oxide (ITO) of liquid crystal display (LCD), removing many current problems such as the image-sticking problem [72].

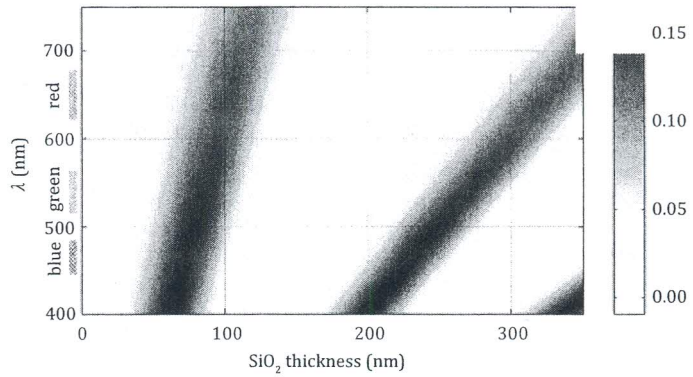

(a)

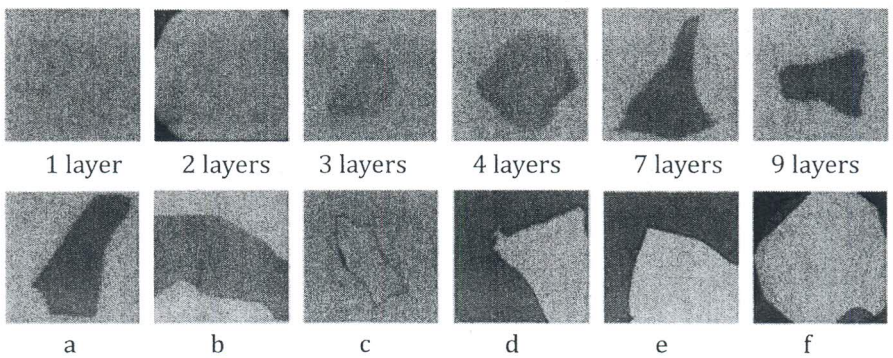

(b)

Figure 6.12 (a) The contrast plotted according to the equation; (b) the contrast shown in the optical images of graphene sheets depending on the number of layers. Pictures a–f are the images of graphene thicker than 10 layers. The number of layers increases from a to f. (Figures (a) and (b) reprinted with permission from ref. 70 and 71, respectively.) See also Color Insert.

While the natural transmission of white light through graphene doesn't depend on the material parameters, graphene also has nonlinear optical properties, allowing different transmission rates when laser pulses of different energy densities are used. It is because the light-electron interaction causes the optical limiting effect of graphene, and this also depends on the environmental refractive index [73]. Wang *et al.* described how thermal heating and ionization of graphene increases the light scattering of graphene. A nonlinear optical reaction brings a better visibility to graphene as it increases the scattering of the incident light. The more intense laser beam is attenuated by graphene, while the weaker ambient light is highly transmitted.

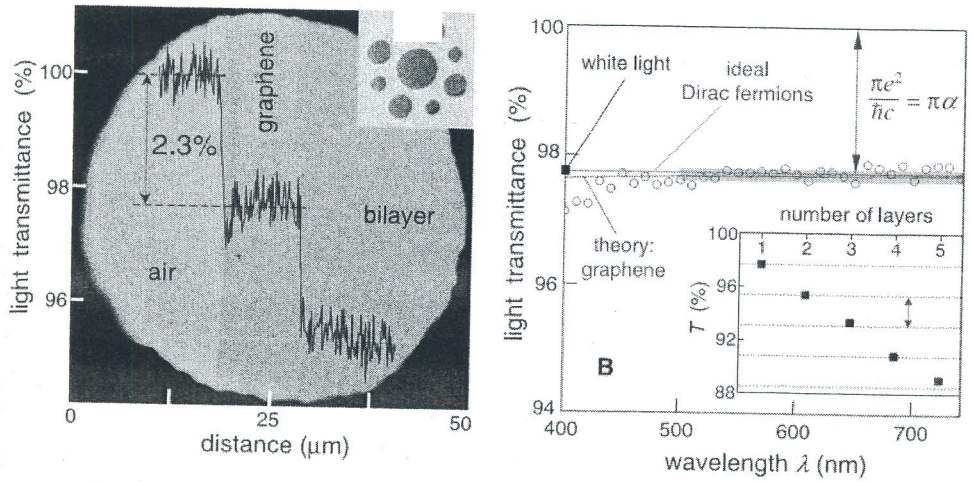

Figure 6.13 (a) An aperture of 50 μm in size was partially covered by a single and bilayer of graphene. The blue line profile indicates the light transmission along the yellow line only dependent on the number of layers; inset — the original sample preparation. (b) A comparison of experimental data of transmission of single-layer graphene (circles) to theoretical expectations of graphene (green line) and ideal Dirac fermion (red line); inset — transmission depending on the number of layers. (Reprinted with permission from ref. 12.) See also Color Insert.

These nonlinear optical properties of graphene originate from nonequilibrium distributions of photoexcited carriers, of which energy is smaller than the optical phonon energy in the low temperature region [74]. This is why the photoresponse of graphene at a long wavelength excitation is strong and its nonlinear response threshold is low. Nonlinear optical properties of graphene can be characterized by the Z-scan method, and the optical-limiting studies on graphene showed that graphene has a nonlinear absorption and scattering with the use of 532 nm and 1064 nm laser pulses (Fig. 6.14).

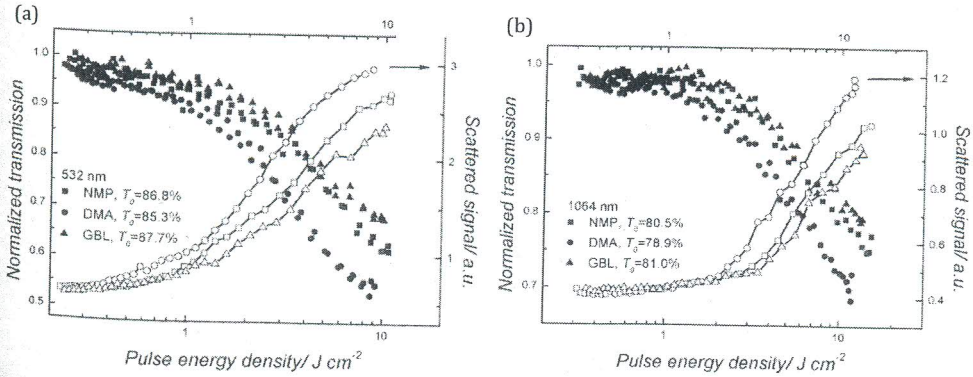

Figure 6.14 Graphene shows nonlinear transmission and scattering in various solvents for (a) 532 nm and (b) 1,064 nm excitations. (Reprinted with permission from ref. 73.)

To ensure the maximum sensitivity of graphene, a single layer of graphene should be confirmed before its application as a sensor. Raman spectroscopy is a very effective method to determine the number of layers [13, 75, 76]. Raman peaks at G′ and G bands show detailed information about the number of graphene layers. The G′ band (sometimes referred to as the "two-dimensional" band) represents the second order of zone-boundary phonons. The neighboring graphene layers interfere with the energy level of the second order of zone-boundary phonons. This results in the splitting and the shift of the G′-band energy level as the number of layers increases. The split and shifted G′-bands are superpositioned to form a characteristic Raman G′ peak (Fig. 6.15).

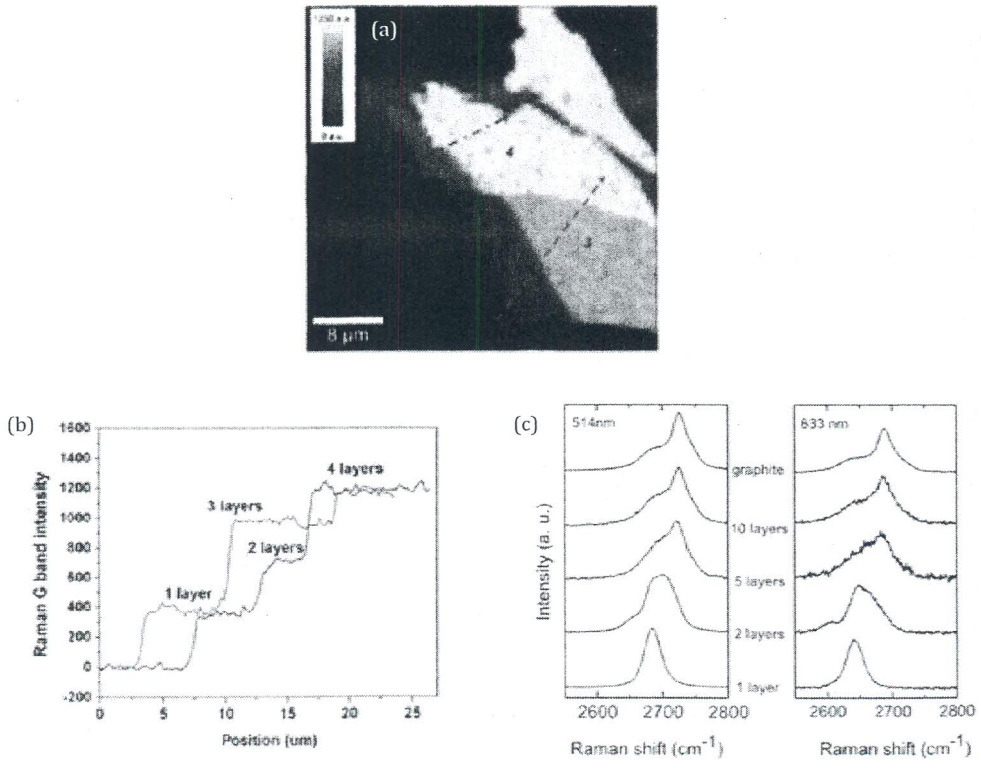

Figure 6.15 (a) Raman-mapping image with respect to the intensity of the G band; (b) the intensity of the G band corresponding to the dash lines in (a); (c) G′ band spectra at 514 nm and 633 nm with different number of layers. (Figures (a) and (b) are reprinted with permission from ref. 72 and (c) is from reprinted with permission from ref. 13.)

Also, Raman spectroscopy can probe the electronic properties via electron-phonon coupling [77], the orientation of graphene edges [78], and the uniaxial tensile stress on strained graphene [79].

Since graphene naturally has a short distance periodicity, it has an excellent response to high-frequency light, which enhances the anisotropy of conductivity. Since the bandgap and photon-induced conduction is suppressed along the zigzag direction of graphene,

high-frequency absorption depends on the polarization of the light. Here, graphene acts like a polarizer [80]. Since this phenomenon depends on the geometry of graphene, it is also sensitive to temperature and physical tension on graphene.

6.3.3 Other Properties

Since electrical and/or optical signals are most commonly measured in sensor operations, we have focused on electrical and optical properties related to graphene. Graphene, in fact, possesses many other extraordinary properties, ranging from chemical [8, 81] and thermal [16] to mechanical. Such properties of graphene could also be relevant for sensing operation or used as sensing mechanisms. Below, we discuss the mechanical properties of graphene and its possible applications in biosensing.

Graphite is composed of a stack of two-dimensional graphene sheets held by van der Waals forces. Lee *et al.* [82] measured the elastic properties and breakdown strength of suspended graphene using an AFM. They found a breaking strength of 42 Nm^{-1} with a corresponding Young's modulus of E = 1.0 TPa. Previous experiments on bulk graphite found a Young's modulus of 1.02 ± 0.03 TPa, while suspended multilayer graphene yields a Young's modulus of 0.5TPa [83]. Therefore, graphene is a very strong and rigid material. These exceptional mechanical properties can be exploited in sensors based on nanoelectromechanical resonators (Fig. 6.16) [17, 84, 85], where high-frequency resonance could be achieved. For any nanoelectromechanical system (NEMS), the resonant frequency depends on the speed of sound on the material $v = \sqrt{E/\rho}$, where E is Young's modulus and ρ is the material density. Compared to Si or gallium arsenide (GaAs), carbon presents the highest value of speed of sound [84] due to a very high value of Young's modulus with a low material density.

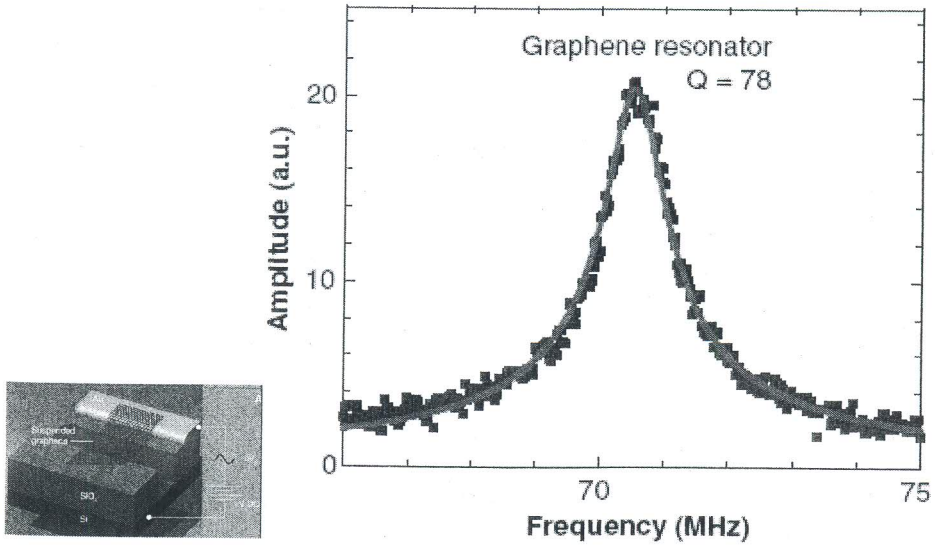

Figure 6.16 The resonance peak of a graphene resonator. The inset shows a scheme of the nanoelectromechanical resonator made from graphene. (Reprinted with permission from ref. 17.)

When a single layer of suspended graphene is used in such a nanoelectromechanical system (NEMS) resonator, a high force sensitivity below 1 fN per root hertz is demonstrated [17]. This sensitivity is suitable for the use of graphene as mass, force, and charge (electrostatic force) sensors. For a resonator, the minimum mass to be detected is:

$$\delta M \sim 2m_{\text{eff}}/Q \times 10^{-\text{DR}/20}$$

Graphene is an excellent choice for mass detector because of its low effective mass. Graphene dynamic range (DR) is sample dependent and is defined as the decibel ratio between the amplitude of onset of nonlinearity to the noise floor. In the supporting material of ref. 17, DR was found to be 60 dB, giving a room temperature mass sensitivity of 450 zeptograms. Such resonators can in principle be used to weigh biomolecules, cells, and nanoparticles in fluids as it was done in ref. 86 by using suspended silicon resonators with microchannels, but the sensitivity can be improved by using graphene (Fig. 6.17).

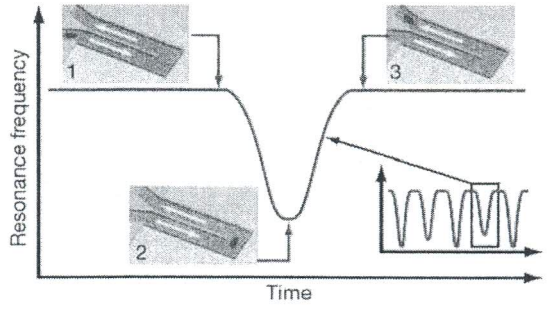

Figure 6.17 Time-dependent resonant frequency while a biomolecule passes through a silicon microchannel cantilever resonator. (Reprinted with permission from ref. 86.)

More parameters such as the quality factor and residual stress need to be manipulated to ensure a precise control on their resonant frequency and minimum mass detection [17, 85]. It was also found [84] that annealing can improve the quality factors in resonators based on graphene and GO.

One of the important properties of graphene is the presence of intrinsic ripples [87] (Fig. 6.18). Ripples in graphene are found to spontaneously appear owing to thermal fluctuations with a size distribution along the peak of approximately 8 nm, which is compatible with experimental findings (5–10 nm) [88]. Ripples are an unavoidable intrinsic property of graphene, stabilizing atomically thin membranes through their deformation in the third dimension and can affect its electronic properties [89].

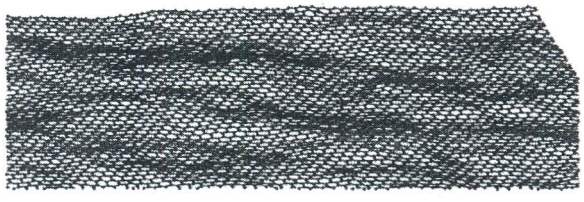

Figure 6.18 A representative configuration of ripples on a graphene surface at 300 K. (Reprinted with permission from ref. 87.)

6.4 Biosensing Applications of Graphene

In this section, we review a number of recent experiments that demonstrate the potential of graphene for sensing applications. Most of these experiments are relevant for biosensors and a few prototypes have been developed.

6.4.1 Electrical Sensing

6.4.1.1 Gas sensing

As mentioned earlier, Schedin *et al.* [10] reported the capability of individual gas molecule detection by graphene FET. The principle of this device is based on changes in the electrical conductivity due to the adsorption of gas molecules on the surface of graphene. The adsorbed molecules change the local carrier concentration acting as donors or acceptors. The unique electronic properties of graphene maximize the sensing effect. Graphene is highly conductive, with a low Johnson noise in the transport measurement. In this experiment, the graphene device was mounted in an evacuated chamber and exposed to a selected chemical diluted in pure helium or nitrogen at atmospheric pressure. The tested chemicals are NO_2, NH_3, H_2O, and CO in concentrations of 1 part per million (ppm). A clear change was detected immediately after letting the chemicals in, followed by saturation (Fig. 6.19).

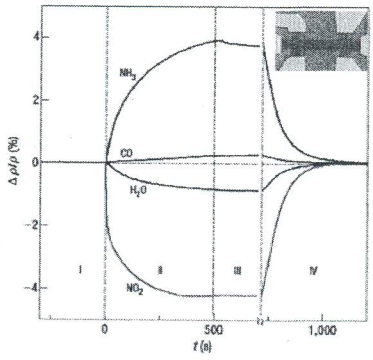

Figure 6.19 Changes in graphene resistivity caused by exposure to various gases (NH_3, CO, H_2O, NO_2) diluted (1 ppm). The positive (negative) sign of changes is due to electron (hole) doping. Region I: the device in vacuum before its exposure to gases; Region II: exposure to a volume of a diluted chemical; Region III: evacuation; Region IV: annealing at 150°C [10]. (Reprinted with permission from ref. 48.)

6.4.1.2 Metal doping

Chen *et al.* [90] reported on the change of electronic characteristics of graphene when potassium atoms are deposited onto its surface in vacuum. The mobility of graphene decreases after more potassium doping. The conductivity versus gate voltage shows the minimum ($V_{g,\,min}$) conductivity shifts to more negative gate voltages for more potassium exposure. Moreover, the researchers tried to dope graphene and changed the position of the Dirac point by the deposition of potassium atoms on a graphene device as shown in Fig. 6.20.

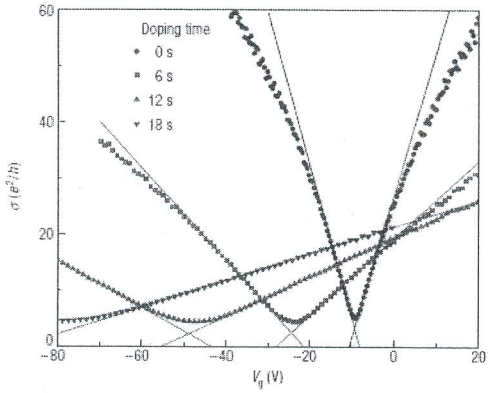

Figure 6.20 Potassium doping of graphene. The conductivity versus gate voltage (V_g) curves for the pristine sample and three different doping concentrations at T = 20 K in UHV. The crossing of the lines defines the points of the residual conductivity and the gate voltage at minimum conductivity ($V_{g,min}$) for each data set. (Reprinted with permission from ref. 47.)

The field effect characteristic is turning more n-type, and the transconductance (proportional to mobility), which can be extracted from the slope of conductance with respect to the back-gate voltage, is being reduced with more deposition of potassium atoms on the graphene device.

6.4.1.3 Chemical and biosensing in electrolytes and other liquids

Graphene shows a high sensing capability in liquid environment. Ohno *et al.* [91] reported electrolyte-gated graphene field-effect transistors (GFETs) for electrically detecting pH and protein adsorptions. In this work, nonfunctionalized graphene was used as a FET channel in an electrolyte. The GFET transconductances was higher in the electrolyte than in vacuum, and the conductance exhibited a direct linear increase with electrolyte pH. The electrical-double layer of electrolyte over the GFET acts as a top-gate insulator with a thickness of 1–5 nm for electrolyte with several millimolars concentration. An Ag/AgCl reference electrode was used as the top-gate electrode. Ambipolar electric field-effect characteristics of a GFET were observed for both back-gate and top-gate operation. Transfer characteristics of GFETs in the electrolyte (e.g., pH 5.8) indicate their high potentials for use in (Fig. 6.21).

Another example of graphene as a pH meter was studied with a few layers of graphene assembled as a solution-gate field-effect transistor (SGFET) with an electrolyte acting as the dietetic [92]. The modulation of the graphene (SGFET channel) conductance was achieved by applying a gate potential from an electrode placed on top of the channel, across the electrolyte. In this experiment one to two or three to four layers epitaxially grown graphene was used to demonstrate pH sensing using cyclic voltammetry (CV) and frequency-dependent impedance spectroscopy of graphene. Frequency-dependent impedance spectroscopy in the potential range from −1.0 V to +1.0 V at frequencies ranging from 5 Hz to 120 Hz shows peaks and a pH-sensitive maxima (Fig. 6.22).

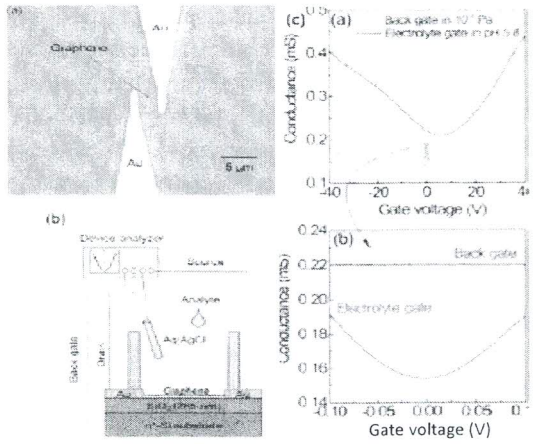

Figure 6.21 GFET-based sensors in an electrolyte. (Reprinted with permission from ref. 91.)

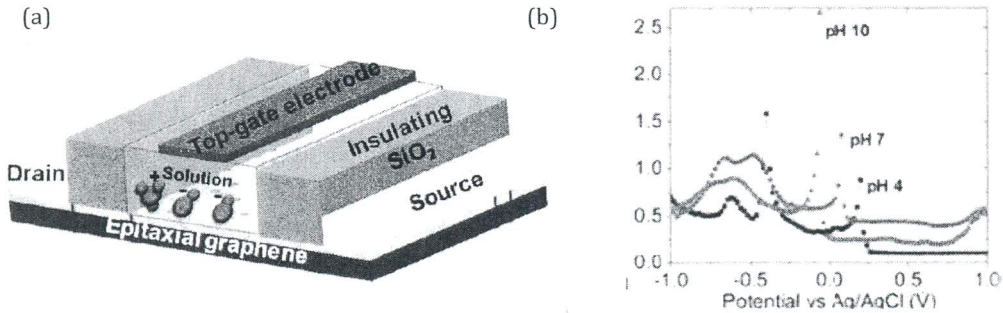

Figure 6.22 (a) A solution-gated epitaxial graphene pH sensor; (b) interfacial capacitance of graphene from impedance measurements. Shown is the pH dependence of interfacial capacitance peak potential (collected at a fixed frequency of 11 Hz). (Reprinted with permission from ref. 92.)

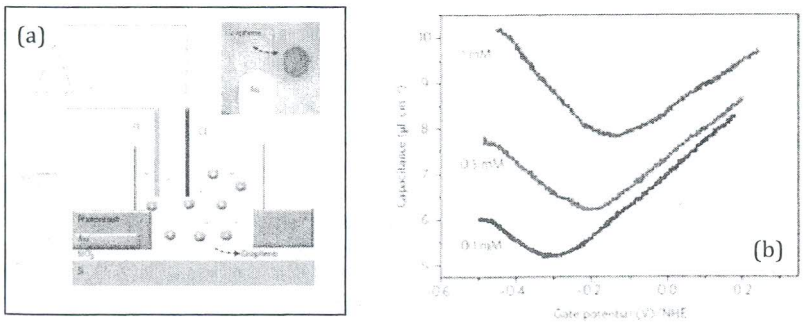

Figure 6.23 (a) A schematic representation of the quantum capacitance measurement setup in which a graphene sheet on a silicon/SiO_2 substrate is connected to a gold electrode; (b) the capacitance of graphene measured in a NaF aqueous solution at different ionic concentrations (0.1 mM, 0.5 mM, and 1 mM, from bottom to top). (Reprinted with permission from ref. 93.)

Chen *et al.* have studied the charge transport in electrochemically gated graphene under different electrolytes, including ionic liquids and aqueous solutions. A double layer is formed above graphene (in the electrochemically gated graphene FET). The double-layer thickness depends on the size of the ions (~1nm). Graphene is able to determine the mobile carrier density in an ionic liquid using a capacitor model, and Chen *et al.* have interpreted the electron transport characteristics in terms of charged impurity–induced scattering [6, 93] (Fig. 6.23).

Shan *et al.* [94] constructed a graphene-based electrochemical biosensor for glucose, which achieved linear glucose response up to 14 mM. These authors also studied the properties of water-soluble graphene covalently functionalized by biocompatible poly-l-lysine [95].

6.4.1.4 Biosensor device

CMG, with a two-dimensional nanostructure and tunable surface chemistry, can interface strongly with the biological systems [19] (Fig. 6.24). The CMGs and their biohybrids can be synthesized using GO, graphene amine (GA), or plasma-modified graphene amine (PGA) immobilized on a silica substrate. PGA was synthesized by exposing the graphite flakes to either ammonia or nitrogen plasma, followed by exfoliation via sonication in water or by exposing the GO sheets on a silica substrate to hydrogen plasma followed by ammonia (or nitrogen) plasma. The GO sheets immobilized on silica were used as templates to selectively and covalently tether single-stranded DNA to build the G-DNA hybrid. Since this DNA's terminal amine group bonds covalently with the carboxylic group on GO and not with the amine groups on silica, the reaction resulted in selective DNA tethering of the GO sheets. The higher DNA density on the surface wrinkles was attributed to the local field enhancement at the sharp edges.

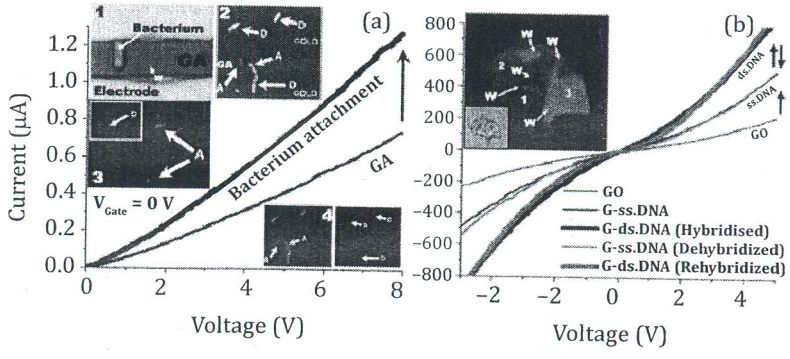

Figure 6.24 (a) The conductivity of the p-type GA device increases upon the attachment of a single bacterial cell. Inset (1–4) show that the bacterium attached to GA on silica remains alive (A); however, the bacteria deposited on the GA atop gold electrodes are dead (D) after electrical measurements. (b) DNA transistor: ss-DNA tethering on GO increases the conductivity of the device. Hybridization and dehybridization of DNA on the G-DNA device result in the reversible increase and restoration of conductivity. Inset shows a G-DNA (ds) sheet with wrinkles and folds clearly visible. (Reprinted with permission from ref. 19.) See also Color Insert.

Graphene-based glucose biosensors have been demonstrated, for example, based on the immobilization of glucose oxidase in platinum nanoparticles/graphene/chitosan nanocomposite film [96] or a oxidase-graphene-chitosan-modified electrode for direct electrochemistry and glucose sensing [97]. Electrochemical sensing and a biosensing platform based on chemically reduced GO have been reported [98]. Understanding the electrochemistry of graphene and related materials have becoming increasingly important for biosensing applications [99, 100].

6.4.2 Optical Sensing

Optical measurements of graphene and/or chemicals bonded to it are useful to confirm a successful modification of graphene. Applications of chemically modified graphene have been studied very intensely because modified graphene is used for many different experiments to detect various molecules. Among them, GO is oxygenated bearing hydroxyl, epoxide, and carbonyl functional groups, and it is very attractive to many researchers for its special properties[42]. Other additional functionalization can be easily equipped, and this strongly implies its possible use in biosensing and drug delivery. Infrared (IR) spectroscopy reveals the existence of –OH, C=O, and C=C bonding of GO [101, 102]. By this method, the further modification of GO, such as GO–PEG for spectral imaging and drug delivery, is verified [103] (Fig. 6.25). This method is especially useful to check the successful chemical modification of graphene for specific detection, applicable for biosensing and drug delivery.

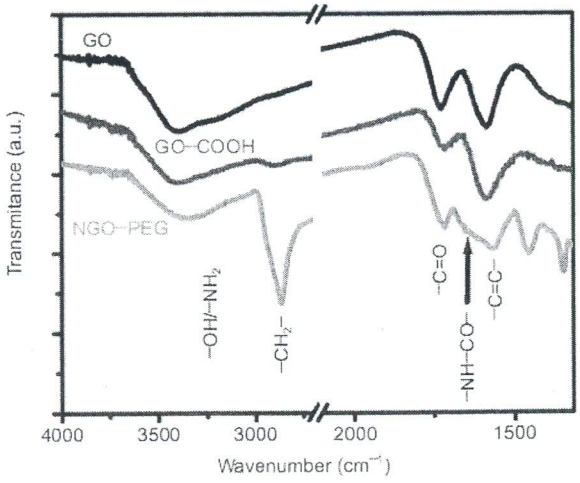

Figure 6.25 IR spectra of chemical bondings on graphene. GO, GO–COOH, and NGO–PEG peaks are seen. (Reprinted with permission from ref. 103.)

Other optical methods are also utilized to study optical properties of graphene and molecules adsorbed to it. UV-Vis-NIR spectroscopy detects the optical absorption peak at 230 nm originated from the π-plasmon of carbon [104]. The more modification to graphene results in a broader absorption bandwidth; GO-COOH and GO-PEG showed much broader bands than GO. Also, the fluorescence of GO excited in the visible range reveals a peak at

570 nm when it is excited by the 400 nm laser, while GO–PEG has a fluorescence peak at 520 nm. Photoluminescence in the IR range also shows the difference between GO and GO-PEG. This is useful in bioimaging because it is almost free from cellular autofluorescence. Recently, it was also shown that graphene-based materials can effectively quench the fluorescence (Fig. 6.26) of other molecules (such as dye molecules) nearby [105, 106] (Fig. 6.26a, b). Lu *et al.* [14] have used GO to sense DNA and proteins based on GO's fluorescence quenching (Fig. 6.26c, d). They demonstrated that the quenched fluorescence can be recovered upon unbinding to as ssDNA from GO caused by the binding of the ssDNA to a target (complementary DNA). Experiments suggesting the biostability of DNA and its protection from cleavage by DNase I (Tang *et al.* 2010]) and DNA-mediated self-assembly of graphene was also demonstrated (Patil *et al.* 2009]. Multicolor fluorescence-based DNA analysis by labeling DNA probes with different fluorophores was later suggested as an improvement (He *et al.* 2010). Molecular beacon–based approaches were also suggested by Lu *et al.* (2010a, b) to detect single-base DNA mismatch *in vitro* and surviving mRNA in cells. Fluorescence resonance energy transfer graphene sensors using quantum dots was demonstrated to detect target DNA (Dong *et al.* 2010) and thrombin (Chang *et al.* 2010). DNA–GO constructs uptake have also been demonstrated in living cells (Wang *et al.* 2010), including drug delivery (Zhang *et al.* 2010). It is clear that graphene could be integrated with fluorescing molecules for both *in vitro* and *in vivo* sensing.

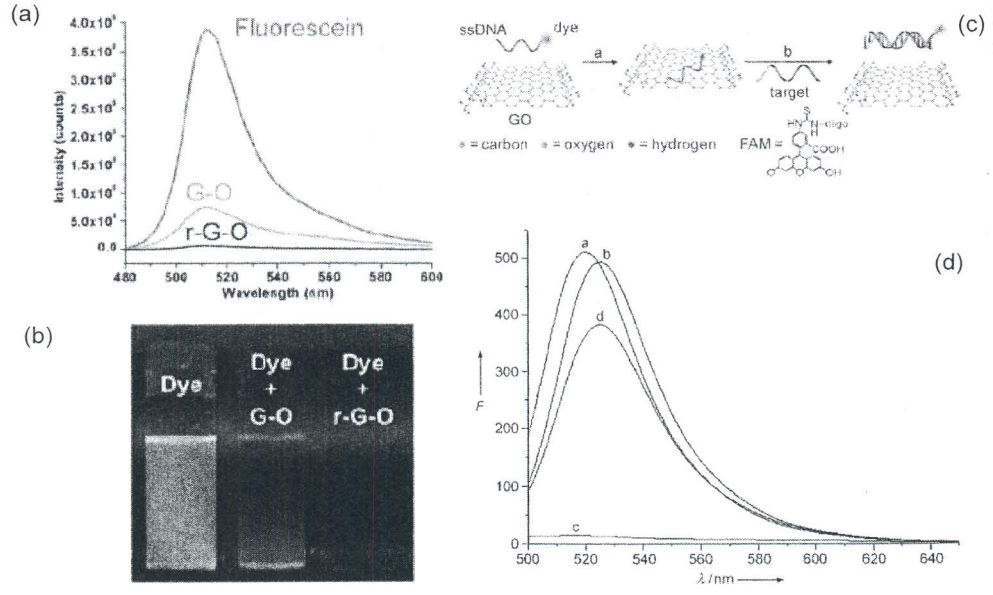

Figure 6.26 (a,b): Fluorescence quenching of dyes due to graphene and GO [38]; (c,d) selective biosensing using GO based on its fluorescence quenching ability [14]; (c) the sensor operation principle; (d) fluorescence emission spectra for a. P1 in Tris-HCl buffer, b. P1 + (300 nM) HIV1, c. P1 + GO, and d. P1 + GO + (300 nM) HIV1 [14]. (Fig. 6.26 a,b and c,d reprinted with permission from ref. 38 and 14, respectively.) See also Color Insert.

Raman spectroscopy is also one of the most useful detection techniques. Raman spectroscopy probes the phonon vibration mode of graphene and electron-phonon interaction. Raman is an excellent tool to monitor the quality of graphene, detecting the charged impurity doping in graphene and defects in graphene [13, 107] and can be sensitive to chemical modifications of graphene [81]. In addition to measuring graphene, one can also probe the Raman spectra of the molecules adsorbed on graphene [15].

Doping and charge impurities in graphene can strongly affect its Raman spectrum. With the existence of doping/charge impurities, the *G* peak is upshifted and its bandwidth is stiffened [77]. *G* peak is upshifted because of Kohn anomaly [108]. Also, the *G* peak is stiffened because phonon decay into electron-hole pairs is blocked by Pauli exclusion. The two-dimensional peak also slightly shifts and, more importantly, its peak intensity strongly varies with the charge impurities. The shift of two-dimensional peak is such that hole-doping induces an upshift and the electron-doping induces a downshift. Lastly, charged impurity doesn't generate the *D* peak while the defects and edges of graphene do [107]. Using this method with Raman spectroscopy, the qualities of graphene and its doping can be monitored [109, 110], with potential applications in biosensing [111].

Not only the Raman spectrum of graphene can be affected by molecules adsorbed on graphene, there are possibilities that graphene may also enhance and affect the Raman spectra of the adsorbed molecules for direct sensing of those molecules through their molecular Raman fingerprints. For example, it has been shown that graphene can enhance (close to 20-fold demonstrated so far) the Raman signals (which would have been unobservable without graphene, e.g., if the molecules are on a Si wafer) of various dye molecules adsorbed on graphene (Fig. 6.27) [15]. The enhancement has been interpreted as due to a chemical mechanism involving the charge transfer between the molecules and graphene. Since the electronic properties of graphene are highly tunable by chemical or electrical (e.g., a gate) manipulations, it would be interesting to explore how such tunability (which, in turn, may influence the charge transfer between graphene and adsorbed molecules) can affect the Raman enhancement and Raman fingerprints of the adsorbed molecules, potentially opening new venues for selective Raman biosensing.

It is worthwhile to point out that in many ways, graphene can be applied for sensing and biosensing as other carbon materials, especially carbon nanotubes, have been. Carbon nanotubes and graphene are both suitable candidate materials for electronic, photonic, and optoelectronic nano-devices and the intense studies on carbon nanotubes, and their sensing applications can often serve as inspirations and/or informative comparison points for applications of graphene. For example, similar to graphene, Raman spectroscopy has been used as a tool to study charge transfer in doped carbon nanotubes [112] and how the direction of carbon nanotube crystals determines its electronic properties [113]. It is also shown that the defects or local environment of SWCNTs can cause different fluorescence spectra emission energy and bandwidth of the nanotubes without fluctuation [114]. The Raman signals of the carbon nanotubes are also sensitive to various chemical modifications, such as oxidization [115]. A carbon nanotube has been used as a Raman label [116] because it generates a strong Raman signal with multiple modifications without photobleaching or quenching. Proteins with the concentration as low as 1 fM could be detected and quantified by this method. Also, gene or drug delivery due to the multifunctionality of carbon nanotubes is a promising application because

graphene protects the gene/drug attached to it until it is released [117, 118]. Moreover, the electronic sensing by carbon nanotubes with special chemical modification is also demonstrated [119]. Most applications listed above can be directly adapted to graphene. Furthermore, the dangling bonds at the edges of a graphene nanoribbon may be chemically functionalized to perform selective biological sensing. The two-dimensional features of graphene can facilitate the application of graphene as a powerful biosensing tool.

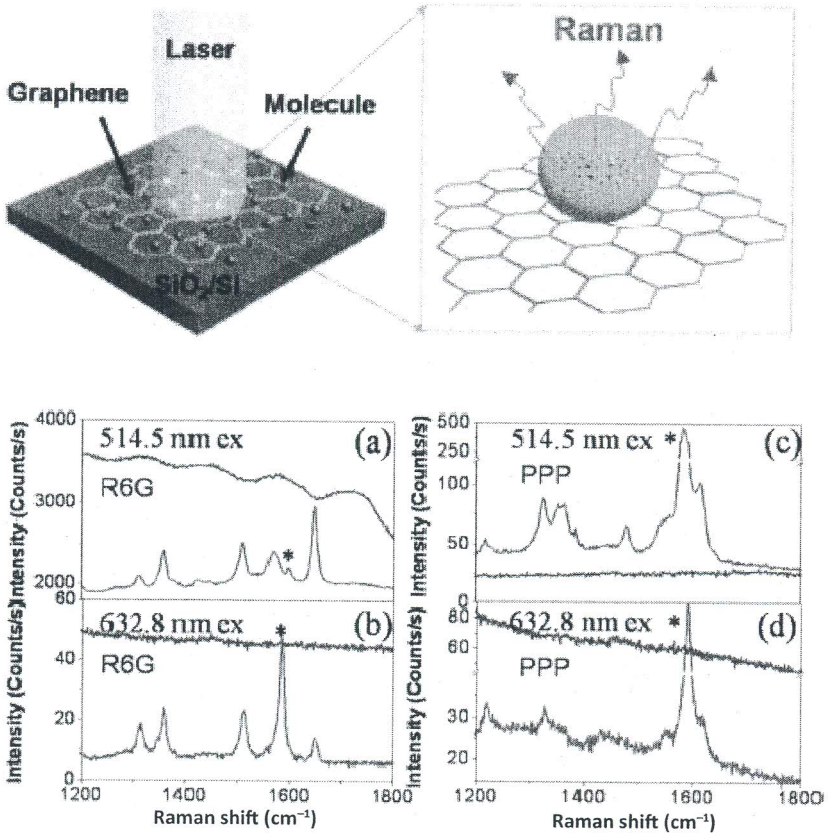

Figure 6.27 The enhancement of the Raman signals of dye molecules on graphene. (Reprinted with permission from ref. 15.)

In addition to sensing experiments, fundamental studies (both experimentally and theoretically) on the interaction of biological molecules, such as DNA/nucleotides, with graphene have been performed [120, 121]. Density functional theory–based methods can be used to model how organic molecules interact with graphene to change its electronic properties [122]. Catalyst-free growth, orientation, and biosensing properties of multilayer graphene nanoflake films with sharp-edged planes have been studied [123]. GO has been found to exhibit peroxidase catalytic activity that could catalyze 3,3,5,5-tetramethylbenzidine (TMB) oxidation with H_2O_2 for glucose detection (Song *et al.* 2010). Liu *et al.* (2010) decorated GO with protein or DNA to fabricate nanoparticle assemblies

on GO as a strategy to synthesize new hybrid materials. We expect that such biomimetic materials could have a variety of functionalities in biomedical sensing.

6.5 Closing Remarks and Future Work

While emphasizing the nature of graphene as a material, the primary focus of this article was on harnessing its potential as a sensor in biological systems. Graphene in biosensing is only at the initial stages. We expect to see an increased thrust in the development of biomimetic graphene materials to address specific cellular functions. Applications *in vivo* will obviously require the development of multifunctional graphene materials that are not cytotoxic while simultaneously enhancing the detection and functional characteristics of the materials, including photothermal therapy. The unparalleled use of graphene in gas sensing will be further advanced to detect volatiles as well as other biothreat agents using integrated portable devices for detecting gaseous compounds in ultralow quantities. While constructing sensor-related applications using graphene and graphene biocomposites, surface fouling and sample presentation steps need to be given careful attention.

References

1. Novoselov, K. S., Geim, A. K., Morozov, S. V., Jiang, D., Zhang, Y., Dubonos, S. V., Grigorieva, I. V., and Firsov, A. A. (2004). Electric field effect in atomically thin carbon films, *Science*, **306**(5696), 666–669.
2. Geim, A. K., and Kim, P. (2008). Carbon wonderland, *Sci. Am.*, **298**(4), 90.
3. Geim, A. K. (2009). Graphene: status and prospects, *Science*, **324**(5934), 1530–1534.
4. Rao, C. N. R., Sood, A. K., Subrahmanyam, K. S., and Govindaraj, A. (2009). Graphene: the new two-dimensional nanomaterial, *Angew. Chem., Int. Ed.*, **48**(42), 7752–7777.
5. Geim, A. K., and Novoselov, K. S. (2007). The rise of graphene, *Nat. Mater.*, **6**(3), 183–191.
6. Chen, F., Qing, Q., Xia, J., Li, J., and Tao, N. (2009). Electrochemical gate-controlled charge transport in graphene in ionic liquid and aqueous solution, *J. Am. Chem. Soc.*, **131**(29), 9908–9909.
7. Stoller, M. D., Park, S., Zhu, Y., An, J., and Ruoff, R. S. (2008). Graphene-based ultracapacitors, *Nano Lett.*, **8**(10), 3498–3502.
8. Park, S., and Ruoff, R. S. (2009). Chemical methods for the production of graphenes, *Nat. Nano*, **4**(4), 217–224.
9. Neto, A. H. C., Guinea, F., Peres, N. M. R., Novoselov, K. S., and Geim, A. K. (2009). The electronic properties of graphene. *Rev. Mod. Phys.*, **81**, 109.
10. Schedin, F., Geim, A. K., Morozov, S. V., Hill, E. W., Blake, P., Katsnelson, M. I., and Novoselov, K. S. (2007). Detection of individual gas molecules adsorbed on graphene, *Nat. Mater.*, **6**(9), 652–655.
11. Li, X., Zhu, Y., Cai, W., Borysiak, M., Han, B., Chen, D., Piner, R. D., Colombo, L., and Ruoff, R. S. (2009). Transfer of large-area graphene films for high-performance transparent conductive electrodes, *Nano Lett.*, **9**(12), 4359–4363.

12. Nair, R. R., Blake, P., Grigorenko, A. N., Novoselov, K. S., Booth, T. J., Stauber, T., Peres, N. M. R., and Geim, A. K. (2008). Fine structure constant defines visual transparency of graphene, *Science*, **320**(5881), 1308.

13. Ferrari, A. C., Meyer, J. C., Scardaci, V., Casiraghi, C., Lazzeri, M., Mauri, F., Piscanec, S., Jiang, D., Novoselov, K. S., Roth, S., and Geim, A. K. (2006). Raman spectrum of graphene and graphene layers, *Phys. Rev. Lett.*, **97**(18), 187401–187404.

14. Chun-Hua, L., Huang-Hao, Y., Chun-Ling, Z., Xi, C., and Guo-Nan, C. (2009). A graphene platform for sensing biomolecules. *Angew. Chem., Int. Ed.*, **48**(26), 4785–4787.

15. Ling, X., Xie, L., Fang, Y., Xu, H., Zhang, H., Kong, J., Dresselhaus, M. S., Zhang, J., and Liu, Z. (2009). Can graphene be used as a substrate for Raman enhancement? *Nano Lett.*, **10**(2), 553–561.

16. Balandin, A. A., Ghosh, S., Bao, W., Calizo, I., Teweldebrhan, D., Miao, F., and Lau, C. N. (2008). Superior thermal conductivity of single-layer graphene, *Nano Lett.*, **8**(3), 902–907.

17. Bunch, J. S., van der Zande, A. M., Verbridge, S. S., Frank, I. W., Tanenbaum, D. M., Parpia, J. M., Craighead, H. G., and McEuen, P. L. (2007). Electromechanical resonators from graphene sheets, *Science*, **315**(5811), 490–493.

18. Lee, C., Wei, X., Kysar, J. W., and Hone, J. (2008). Measurement of the elastic properties and intrinsic strength of monolayer graphene, *Science*, **321**(5887), 385–388.

19. Mohanty, N., and Berry, V. (2008). Graphene-based single-bacterium resolution biodevice and DNA transistor: interfacing graphene derivatives with nanoscale and microscale biocomponents, *Nano Lett.*, **8**(12), 4469–4476.

20. Novoselov, K. S., Jiang, D., Schedin, F., Booth, T. J., Khotkevich, V. V., Morozov, S. V., and Geim, A. K. (2005). Two-dimensional atomic crystals, *Proc. Natl. Acad. Sci. USA*, **102**(30), 10451–10453.

21. Liang, X., Fu, Z., and Chou, S. Y. (2007). Graphene transistors fabricated via transfer-printing in device active-areas on large wafer, *Nano Lett.*, **7**(12), 3840–3844.

22. Berger, C., Song, Z., Li, X., Wu, X., Brown, N., Naud, C., Mayou, D., Li, T., Hass, J., Marchenkov, A. N., Conrad, E. H., First, P. N., and de Heer, W. A. (2006). Electronic confinement and coherence in patterned epitaxial graphene, *Science*, **312**(5777), 1191–1196.

23. Li, X., Cai, W., An, J., Kim, S., Nah, J., Yang, D., Piner, R., Velamakanni, A., Jung, I., Tutuc, E., Banerjee, S. K., Colombo, L., and Ruoff, R. S. (2009). Large-area synthesis of high-quality and uniform graphene films on copper foils, *Science*, **324**(5932), 1312–1314.

24. Wintterlin, J., and Bocquet, M. L. (2009). Graphene on metal surfaces, *Surf. Sci.*, **603**(10–12), 1841–1852.

25. Anton, N. S., Mehdi, M. Y., Romaneh, J., Ouseph, P. J., Cohn, R. W., and Sumanasekera, G. U. (2007). Electrostatic deposition of graphene, *Nanotechnology*, (13), 135301.

26. Liang, X., Chang, A. S. P., Zhang, Y., Harteneck, B. D., Choo, H., Olynick, D. L., and Cabrini, S. (2009). Electrostatic force assisted exfoliation of prepatterned few-layer graphenes into device sites. *Nano Lett.*, **9**(1), 467–472.

27. Hernandez, Y., Nicolosi, V., Lotya, M., Blighe, F. M., Sun, Z., De, S., McGovern, I. T., Holland, B., Byrne, M., Gun'Ko, Y. K., Boland, J. J., Niraj, P., Duesberg, G., Krishnamurthy, S., Goodhue, R., Hutchison, J., Scardaci, V., Ferrari, A. C., and Coleman, J. N. (2008). High-yield production of graphene by liquid-phase exfoliation of graphite, *Nat. Nano*, **3**(9), 563–568.

28. Li, X., Wang, X., Zhang, L., Lee, S., and Dai, H. (2008). Chemically derived, ultrasmooth graphene nanoribbon semiconductors, *Science*, **319**(5867), 1229–1232.

29. de Heer, W. A., Berger, C., Wu, X., First, P. N., Conrad, E. H., Li, X., Li, T., Sprinkle, M., Hass, J., Sadowski, M. L., Potemski, M., and Martinez, G. (2007). Epitaxial graphene, *Solid State Commun.*, **143**(1–2), 92–100.
30. Emtsev, K. V., Bostwick, A., Horn, K., Jobst, J., Kellogg, G. L., Ley, L., McChesney, J. L., Ohta, T., Reshanov, S. A., Rohrl, J., Rotenberg, E., Schmid, A. K., Waldmann, D., Weber, H. B., and Seyller, T. (2009). Towards wafer-size graphene layers by atmospheric pressure graphitization of silicon carbide, *Nat. Mater.*, **8**(3), 203–207.
31. Chuhei, O., and Ayato, N. (1997). Ultra-thin epitaxial films of graphite and hexagonal boron nitride on solid surfaces, *J. Phys.: Condens. Matter*, (1), 1.
32. Cao, H., Yu, Q., Jauregui, L. A., Tian, J., Wu, W., Liu, Z., Jalilian, R., Benjamin, D. K., Jiang, Z., and Bao, J. (2009). Wafer-scale graphene synthesized by chemical vapor deposition at ambient pressure, *Appl. Phys. Lett.*, **96**, 122106.
33. Bae, S., Kim, H. K., Xu, X., Balakrishnan, J., Lei, T., Song, Y. I., Kim, Y. J., Ozyilmaz, B., Ahn, J. H., and Hong, B. H. (2009). 30-inch roll-based production of high-quality graphene films for flexible transparent electrodes, *Nat. Nanotechnol.*, **5**, 574–578.
34. Yu, Q., Lian, J., Siriponglert, S., Li, H., Chen, Y., and Pei, S.-S. (2008). Graphene synthesis by surface segregation on Ni and Cu, *Arxiv preprint arXiv:0804.1778v1*.
35. Levendorf, M. P., Ruiz-Vargas, C. S., Garg, S., and Park, J. (2009). Transfer-free batch fabrication of single layer graphene transistors, *Nano Lett.*, **9**(12), 4479–4483.
36. Yu, Q., Lian, J., Siriponglert, S., Li, H., Chen, Y. P., and Pei, S.-S. (2008). Graphene segregated on Ni surfaces and transferred to insulators, *Appl. Phys. Lett.*, **93**(11), 113103–113105.
37. Cao, H., Yu, Q., Pandey, D., Zemlianov, D., Colby, R., Childres, I., Drachev, V., Stach, E., Lian, J., and Li, H. (2009). Large scale graphene films synthesized on metals and transferred to insulators for electronic applications, *Adv. Mater.*, **107**(4), 1–15.
38. Kim, K. S., Zhao, Y., Jang, H., Lee, S. Y., Kim, J. M., Kim, K. S., Ahn, J.-H., Kim, P., Choi, J.-Y., and Hong, B. H. (2009). Large-scale pattern growth of graphene films for stretchable transparent electrodes, *Nature*, **457**(7230), 706–710.
39. Reina, A., Jia, X., Ho, J., Nezich, D., Son, H., Bulovic, V., Dresselhaus, M. S., and Kong, J. (2009). Layer area, few-layer graphene films on arbitrary substrates by chemical vapor deposition, *Nano Lett.*, **9**(8), 3087–3087.
40. Gilje, S., Han, S., Wang, M., Wang, K. L., and Kaner, R. B. (2007). A chemical route to graphene for device applications, *Nano Lett.*, **7**(11), 3394–3398.
41. Gomez-Navarro, C., Weitz, R. T., Bittner, A. M., Scolari, M., Mews, A., Burghard, M., and Kern, K. (2007). Electronic transport properties of individual chemically reduced graphene oxide sheets, *Nano Lett.*, **7**(11), 3499–3503.
42. Stankovich, S., Dikin, D. A., Dommett, G. H. B., Kohlhaas, K. M., Zimney, E. J., Stach, E. A., Piner, R. D., Nguyen, S. T., and Ruoff, R. S. (2006). Graphene-based composite materials, *Nature*, **442**(7100), 282–286.
43. Datta, S. (2005). *Quantum Transport: Atom to Transistor*, 2nd edn, Cambridge University Press, Cambridge, UK.
44. Zhang, Y. B., Tan, Y. W., Stormer, H. L., and Kim, P. (2005). Experimental observation of the quantum Hall effect and Berry's phase in graphene, *Nature*, **438**(7065), 201–204.
45. Purewal, M. S., Hong, B. H., Ravi, A., Chandra, B., Hone, J., and Kim, P. (2007). Scaling of resistance and electron mean free path of single-walled carbon nanotubes, *Phys. Rev. Lett.*, **98**(18), 4.

46. Geim, A. K., and Novoselov, K. S. (2007). The rise of graphene. *Nat. Mater.*, **6**(3), 183–191.
47. Chen, J. H., Jang, C., Adam, S., Fuhrer, M. S., Williams, E. D., and Ishigami, M. (2008). Charged-impurity scattering in graphene, *Nat. Phys.*, **4**(5), 377–381.
48. Schedin, F., Geim, A. K., Morozov, S. V., Hill, E. W., Blake, P., Katsnelson, M. I., and Novoselov, K. S. (2007). Detection of individual gas molecules adsorbed on graphene, *Nat. Mater.*, **6**(9), 652–655.
49. Novoselov, K. S., Geim, A. K., Morozov, S. V., Jiang, D., Katsnelson, M. I., Grigorieva, I. V., Dubonos, S. V., and Firsov, A. A. (2005). Two-dimensional gas of massless Dirac fermions in graphene, *Nature*, **438**(7065), 197–200.
50. Lin, Y.-M., and Avouris, P. (2008). Strong suppression of electrical noise in bilayer graphene nanodevices. *Nano Lett.*, **8**(8), 2119–2125.
51. Bolotin, K. I., Sikes, K. J., Jiang, Z., Klima, M., Fudenberg, G., Hone, J., Kim, P., and Stormer, H. L. (2008). Ultrahigh electron mobility in suspended graphene, *Solid State Commun.*, **146**(9–10), 351–355.
52. Du, X., Skachko, I., Barker, A., and Andrei, E. Y. (2008). Approaching ballistic transport in suspended graphene, *Nat. Nanotechnol.*, **3**(8), 491–495.
53. Tan, Y. W., Zhang, Y., Stormer, H. L., and Kim, P. (2007). Temperature dependent electron transport in graphene, *Eur. Phys. J.*, **148**, 15–18.
54. Bolotin, K. I., Sikes, K. J., Hone, J., Stormer, H. L., and Kim, P. (2008). Temperature-dependent transport in suspended graphene, *Phys. Rev. Lett.*, **101**(9), 096802.
55. Chen, J.-H., Cullen, W. G., Jang, C., Fuhrer, M. S., and Williams, E. D. (2009). Defect scattering in graphene, *Phys. Rev. Lett.*, **102**(23), 236805.
56. Bolotin, K. I., Sikes, K. J., Hone, J., Stormer, H. L., and Kim, P. (2008). Temperature-dependent transport in suspended graphene, *Phys. Rev. Lett.*, **101**(9), 4.
57. Tan, Y. W., Zhang, Y., Stormer, H. L., and Kim, P. (2007). Temperature dependent electron transport in graphene, *Eur. Phys. J. Spec. Top.*, **148**(1), 15–18.
58. Han, M. Y., Özyilmaz, B., Zhang, Y., and Kim, P. (2007). Energy band-gap engineering of graphene nanoribbons, *Phys. Rev. Lett.*, **98**(20), 206805.
59. Pedersen, T. G., Flindt, C., Pedersen, J., Jauho, A.-P., Mortensen, N. A., and Pedersen, K. (2008). Optical properties of graphene antidot lattices, *Phys. Rev. B: Condens. Matter Mater. Phys.*, **77**(24), 245431–245436.
60. Oostinga, J. B., Heersche, H. B., Liu, X., Morpurgo, A. F., and Vandersypen, L. M. K. (2008). Gate-induced insulating state in bilayer graphene devices, *Nat. Mater.*, **7**(2), 151–157.
61. Zhou, S. Y., Gweon, G. H., Fedorov, A. V., First, P. N., de Heer, W. A., Lee, D. H., Guinea, F., Castro Neto, A. H., and Lanzara, A. (2007). Substrate-induced bandgap opening in epitaxial graphene, *Nat. Mater.*, **6**(10), 770–775.
62. Wu, X., Sprinkle, M., Li, X., Ming, F., Berger, C., and de Heer, W. A. (2008). Epitaxial-graphene/graphene-oxide junction: an essential step towards epitaxial graphene electronics, *Phys. Rev. Lett.*, **101**(2), 026801.
63. Barone, V., Hod, O., and Scuseria, G. E. (2006). Electronic structure and stability of semiconducting graphene nanoribbons, *Nano Lett.*, **6**(12), 2748–2754.
64. Han, M. Y., Ozyilmaz, B., Zhang, Y. B., and Kim, P. (2007). Energy band-gap engineering of graphene nanoribbons, *Phys. Rev. Lett.*, **98**(20), 4.

65. Chen, Z. H., Lin, Y. M., Rooks, M. J., and Avouris, P. (2007). Graphene nano-ribbon electronics, *Physica E*, **40**(2), 228–232.

66. Oostinga, J. B., Heersche, H. B., Liu, X. L., Morpurgo, A. F., and Vandersypen, L. M. K. (2008). Gate-induced insulating state in bilayer graphene devices, *Nat. Mater.*, **7**(2), 151–157.

67. Zhou, S. Y., Gweon, G. H., Fedorov, A. V., First, P. N., De Heer, W. A., Lee, D. H., Guinea, F., Neto, A. H. C., and Lanzara, A. (2007). Substrate-induced bandgap opening in epitaxial graphene, *Nat. Mater.*, **6**(10), 770–775.

68. Abergel, D. S. L., Russell, A., and Fal'ko, V. I. (2007). Visibility of graphene flakes on a dielectric substrate, *Appl. Phys. Lett.*, **91**(6), 063125–063127.

69. Avouris, P., Chen, Z., and Perebeinos, V. (2007). Carbon-based electronics, *Nat. Nano*, **2**(10), 605–615.

70. Blake, P., Hill, E. W., Neto, A. H. C., Novoselov, K. S., Jiang, D., Yang, R., Booth, T. J., and Geim, A. K. (2007). Making graphene visible, *Appl. Phys. Lett.*, **91**(6), 063124–063126.

71. Ni, Z. H., Wang, H. M., Kasim, J., Fan, H. M., Yu, T., Wu, Y. H., Feng, Y. P., and Shen, Z. X. (2007). Graphene thickness determination using reflection and contrast spectroscopy, *Nano Lett.*, **7**(9), 2758–2763.

72. Blake, P., Brimicombe, P. D., Nair, R. R., Booth, T. J., Jiang, D., Schedin, F., Ponomarenko, L. A., Morozov, S. V., Gleeson, H. F., Hill, E. W., Geim, A. K., and Novoselov, K. S. (2008). Graphene-based liquid crystal device, *Nano Lett.*, **8**(6), 1704–1708.

73. Jun, W., Yenny, H., Mustafa, L., Jonathan, N. C., and Werner, J. B. (2009). Broadband nonlinear optical response of graphene dispersions, *Adv. Mater.*, **21**(23), 2430–2435.

74. Vasko, F. T., and Ryzhii, V. (2008). Photoconductivity of intrinsic graphene, *Phys. Rev. B: Condens. Matter Mater. Phys.*, **77**(19), 195433–195440.

75. Graf, D., Molitor, F., Ensslin, K., Stampfer, C., Jungen, A., Hierold, C., and Wirtz, L. (2007). Spatially resolved Raman spectroscopy of single- and few-layer graphene, *Nano Lett.*, **7**(2), 238–242.

76. Gupta, A., Chen, G., Joshi, P., and Tadigadapa, S. (2006). Eklund, Raman scattering from high-frequency phonons in supported n-graphene layer films, *Nano Lett.*, **6**(12), 2667–2673.

77. Yan, J., Zhang, Y., Kim, P., and Pinczuk, A. (2007). Electric field effect tuning of electron-phonon coupling in graphene, *Phys. Rev. Lett.*, **98**(16), 166802.

78. Casiraghi, C., Hartschuh, A., Qian, H., Piscanec, S., Georgi, C., Fasoli, A., Novoselov, K. S., Basko, D. M., and Ferrari, A. C. (2009). Raman spectroscopy of graphene edges, *Nano Lett.*, **9**(4), 1433–1441.

79. Huang, M., Yan, H., Chen, C., Song, D., Heinz, T. F., and Hone, J. (2009). Phonon softening and crystallographic orientation of strained graphene studied by Raman spectroscopy, *Proc. Natl. Acad. Sci. USA*, **106**(18), 7304–7308.

80. Zhang, C., Chen, L., and Ma, Z. (2008). Orientation dependence of the optical spectra in graphene at high frequencies, *Phys. Rev. B: Condens. Matter Mater. Phys.*, **77**(24), 241402–4.

81. Elias, D. C., Nair, R. R., Mohiuddin, T. M. G., Morozov, S. V., Blake, P., Halsall, M. P., Ferrari, A. C., Boukhvalov, D. W., Katsnelson, M. I., Geim, A. K., and Novoselov, K. S. (2009). Control of graphene's properties by reversible hydrogenation: evidence for graphane, *Science*, **323**(5914), 610–613.

82. Lee, C., Wei, X. D., Kysar, J. W., and Hone, J. (2008). Measurement of the elastic properties and intrinsic strength of monolayer graphene, *Science*, **321**(5887), 385–388.

83. Frank, I. W., Tanenbaum, D. M., Van der Zande, A. M., and McEuen, P. L. (2007). Mechanical properties of suspended graphene sheets, *J. Vac. Sci. Technol., B: Microelectron. Nanometer Struct.*, **6**, 2558–2561.

84. Robinson, J. T., Zalalutdinov, M., Baldwin, J. W., Snow, E. S., Wei, Z. Q., Sheehan, P., and Houston, B. H. (2008). Wafer-scale reduced graphene oxide films for nanomechanical devices, *Nano Lett.*, **8**(10), 3441–3445.

85. Shivaraman, S., Barton, R. A., Yu, X., Alden, J., Herman, L., Chandrashekhar, M. V. S., Park, J., McEuen, P. L., Parpia, J. M., Craighead, H. G., and Spencer, M. G. (2009). Free-standing epitaxial graphene, *Nano Lett.*, **9**(9), 3100–3105.

86. Burg, T. P., Godin, M., Knudsen, S. M., Shen, W., Carlson, G., Foster, J. S., Babcock, K., and Manalis, S. R. (2007). Weighing of biomolecules, single cells and single nanoparticles in fluid, *Nature*, **446**(7139), 1066–1069.

87. Fasolino, A., Los, J. H., and Katsnelson, M. I. (2007). Intrinsic ripples in graphene, *Nat. Mater.*, **6**(11), 858–861.

88. Meyer, J. C., Geim, A. K., Katsnelson, M. I., Novoselov, K. S., Booth, T. J., and Roth, S. (2007). The structure of suspended graphene sheets, *Nature*, **446**(7131), 60–63.

89. Morozov, S. V., Novoselov, K. S., Katsnelson, M. I., Schedin, F., Elias, D. C., Jaszczak, J. A., and Geim, A. K. (2008). Giant intrinsic carrier mobilities in graphene and its bilayer, *Phys. Rev. Lett.*, **100**(1), 016602–016605.

90. Chen, J.-H., Jang, C., Xiao, S., Ishigami, M., and Fuhrer, M. S. (2008). Intrinsic and extrinsic performance limits of graphene devices on SiO2, *Nat. Nano*, **3**(4), 206–209.

91. Ohno, Y., Maehashi, K., Yamashiro, Y., and Matsumoto, K. (2009). Electrolyte-gated graphene field-effect transistors for detecting pH and protein adsorption, *Nano Lett.*, **9**(9), 3318–3322.

92. Ang, P. K., Chen, W., Wee, A. T. S., and Loh, K. P. (2008). Solution-gated epitaxial graphene as pH sensor, *J. Am. Chem. Soc.*, **130**(44), 14392–14393.

93. Xia, J., Chen, F., Li, J., and Tao, N. (2009). Measurement of the quantum capacitance of graphene, *Nat Nano*, **4**, 505–509.

94. Shan, C., Yang, H., Song, J., Han, D., Ivaska, A., and Niu, L. (2009). Direct electrochemistry of glucose oxidase and biosensing for glucose based on graphene, *Anal. Chem.*, **81**(6), 2378–2382.

95. Shan, C., Yang, H., Han, D., Zhang, Q., Ivaska, A., and Niu, L. (2009). Water-soluble graphene covalently functionalized by biocompatible poly-l-lysine, *Langmuir*, **25**(20), 12030–12033.

96. Wu, H., Wang, J., Kang, X., Wang, C., Wang, D., Liu, J., Aksay, I. A., and Lin, Y. (2009). Glucose biosensor based on immobilization of glucose oxidase in platinum nanoparticles/graphene/chitosan nanocomposite film, *Talanta*, **80**(1), 403–406.

97. Kang, X., Wang, J., Wu, H., Aksay, I. A., Liu, J., and Lin, Y. (2009). Glucose oxidase-graphene-chitosan modified electrode for direct electrochemistry and glucose sensing, *Biosens. Bioelectron.*, **25**(4), 901–905.

98. Zhou, M., Zhai, Y., and Dong, S. (2009). Electrochemical sensing and biosensing platform based on chemically reduced graphene oxide, *Anal. Chem.*, **81**(14), 5603–5613.

99. Alwarappan, S., Erdem, A., Liu, C., and Li, C.-Z. (2009). Probing the Electrochemical Properties of Graphene Nanosheets for Biosensing Applications. *The Journal of Physical Chemistry C*, **113**(20), 8853–8857.

100. Martin, P. (2009). Electrochemistry of graphene: new horizons for sensing and energy storage, *Chem. Rec.*, **9**(4), 211–223.

101. Hontoria-Lucas, C., López-Peinado, A. J., López-González, J. d. D., Rojas-Cervantes, M. L., and Martín-Aranda, R. M. (1995). Study of oxygen-containing groups in a series of graphite oxides: physical and chemical characterization. *Carbon*, **33**(11), 1585–1592.

102. Szabó, T., Berkesi, O., and Dékány, I. (2005). DRIFT study of deuterium-exchanged graphite oxide, *Carbon*, **43**(15), 3186–3189.

103. Sun, X., Liu, Z., Welsher, K., Robinson, J. T., Goodwin, A., Zaric, S., and Dai, H. (2008). Nano-graphene oxide for cellular imaging and drug delivery, *Nano Res.*, **1**(3), 203–212.

104. Attal, S., Thiruvengadathan, R., and Regev, O. (2006). Determination of the concentration of single-walled carbon nanotubes in aqueous dispersions using UV-visible absorption spectroscopy, *Anal. Chem.*, **78**(23), 8098–8104.

105. Kim, J., Cote, L. J., Kim, F., and Huang, J. (2009). Visualizing graphene based sheets by fluorescence quenching microscopy, *J. Am. Chem. Soc.*, **132**(1), 260–267.

106. Xie, L., Ling, X., Fang, Y., Zhang, J., and Liu, Z. (2009). Graphene as a substrate to suppress fluorescence in resonance Raman spectroscopy, *J. Am. Chem. Soc.*, **131**(29), 9890–9891.

107. Casiraghi, C., Pisana, S., Novoselov, K. S., Geim, A. K., and Ferrari, A. C. (2007). Raman fingerprint of charged impurities in graphene, *Appl. Phys. Lett.*, **91**(23), 233108–233110.

108. Pisana, S., Lazzeri, M., Casiraghi, C., Novoselov, K. S., Geim, A. K., Ferrari, A. C., and Mauri, F. (2007). Breakdown of the adiabatic born-Oppenheimer approximation in graphene, *Nat. Mater.*, **6**(3), 198–201.

109. Das, A., Pisana, S., Chakraborty, B., Piscanec, S., Saha, S. K., Waghmare, U. V., Novoselov, K. S., Krishnamurthy, H. R., Geim, A. K., Ferrari, A. C., and Sood, A. K. (2008). Monitoring dopants by Raman scattering in an electrochemically top-gated graphene transistor, *Nat. Nano*, **3**(4), 210–215.

110. Xiaochen, D., Dongliang, F., Wenjing, F., Yumeng, S., Peng, C., and Lain-Jong, L. (2009). Doping single-layer graphene with aromatic molecules, *Small*, **5**(12), 1422–1426.

111. Das, B., Voggu, R., Rout, C. S., and Rao, C. N. R. (2008). Changes in the electronic structure and properties of graphene induced by molecular charge-transfer, *Chem. Commun.*, (41), 5155–5157.

112. Rao, A. M., Eklund, P. C., Bandow, S., Thess, A., and Smalley, R. E. (1997). Evidence for charge transfer in doped carbon nanotube bundles from Raman scattering, *Nature*, **388**(6639), 257–259.

113. Jorio, A., Saito, R., Hafner, J. H., Lieber, C. M., Hunter, M., McClure, T., Dresselhaus, G., and Dresselhaus, M. S. (2001). Structural (n, m) determination of isolated single-wall carbon nanotubes by resonant Raman scattering, *Phys. Rev. Lett.*, **86**(6), 1118.

114. Hartschuh, A., Pedrosa, H. N., Novotny, L., and Krauss, T. D. (2003). Simultaneous fluorescence and Raman scattering from single carbon nanotubes, *Science*, **301**(5638), 1354–1356.

115. Christian, S., Carola, M., and Claus, M. S. (2008). Oxidation induced shifts of Raman modes of carbon nanotubes, *Phys. Status Solidi B*, **245**(10), 2205–2208.

116. Chen, Z., Tabakman, S. M., Goodwin, A. P., Kattah, M. G., Daranciang, D., Wang, X., Zhang, G., Li, X., Liu, Z., Utz, P. J., Jiang, K., Fan, S., and Dai, H. (2008). Protein microarrays with carbon nanotubes as multicolor Raman labels, *Nat. Biotech.*, **26**(11), 1285–1292.

117. Prato, M., Kostarelos, K., and Bianco, A. (2008). Functionalized carbon nanotubes in drug design and discovery, *Acc. Chem. Res.*, **41**(1), 60–68.

118. Wu, Y., Phillips, J. A., Liu, H., Yang, R., and Tan, W. (2008). Carbon nanotubes protect DNA strands during cellular delivery, *ACS Nano*, **2**(10), 2023–2028.

119. Martinez, M. T., Tseng, Y.-C., Ormategui, N., Loinaz, I., Eritja, R., and Bokor, J. (2009). Label-free DNA biosensors based on functionalized carbon nanotube field effect transistors, *Nano Lett.*, **9**, 530–536.

120. Gowtham, S., Scheicher, R. H., Ahuja, R., Pandey, R., and Karna, S. P. (2007). Physisorption of nucleobases on graphene: density-functional calculations, *Phys. Rev. B: Condens. Matter Mater. Phys.*, **76**(3), 033401–033404.

121. Neenu, V., Umesha, M., Achutharao, G., Anindya, D., Prabal, K. M., Ajay, K. S., and Rao, C. N. R. (2009). Binding of DNA nucleobases and nucleosides with graphene, *Chem. Phys. Chem.*, **10**(1), 206–210.

122. Lu, Y. H., Chen, W., Feng, Y. P., and He, P. M. (2009). Tuning the electronic structure of graphene by an organic molecule, *J. Phys. Chem. B*, **113**(1), 2–5.

123. Nai Gui, S., Pagona, P., Martin, M., Ming, C., Artemis, S., Alessandro, P., Sarnjeet, S. D., and Helder, M. (2008). Catalyst-free efficient growth, orientation and biosensing properties of multilayer graphene nanoflake films with sharp edge planes, *Adv. Funct. Mater.*, **18**(21), 3506–3514.